# Stage-discharge rating curves based on satellite altimetry and modeled discharge in the Amazon basin

Adrien Paris, Rodrigo Dias de Paiva, Joecila Santos da Silva, Daniel Medeiros Moreira, Stéphane Calmant, Pierre-André Garambois, Walter Collischonn, Marie-Paule Bonnet, F. Seyler

HAL Id: hal-02136144
https://hal.science/hal-02136144

Submitted on 5 Nov 2019

# Stage-discharge rating curves based on satellite altimetry and modeled discharge in the Amazon basin

**Adrien Paris[1,2,3], Rodrigo Dias de Paiva[1], Joecila Santos da Silva[3,4], Daniel Medeiros Moreira[2,3,5], Stephane Calmant[2,3], Pierre-André Garambois[6], Walter Collischonn[1,3], Marie-Paule Bonnet[3,7], and Frederique Seyler[3,8]**

[1]IPH/UFRGS, Avenida Bento Gonçalves, Porto Alegre, Rio Grande do Sul, Brazil, [2]LEGOS, Université de Toulouse, CNRS, CNES, IRD, UPS, Toulouse, France, [3]LMI OCE IRD/UNB Campus Darcy Ribeiro, Brasilia, Brazil, [4]CESTU/UEA, Manaus, Brazil, [5]UFRJ/CPRM, Rio de Janeiro, Brazil, [6]INSA Strasbourg, ICUBE–UMR7357, Fluid Mechanics Team, Strasbourg, France, [7]UMR5563 GET/IRD/OMP, Toulouse, France, [8]UMR 228, Espace-DEV, IRD, Cayenne, French Guyana

**Abstract** In this study, rating curves (RCs) were determined by applying satellite altimetry to a poorly gauged basin. This study demonstrates the synergistic application of remote sensing and watershed modeling to capture the dynamics and quantity of flow in the Amazon River Basin, respectively. Three major advancements for estimating basin-scale patterns in river discharge are described. The first advancement is the preservation of the hydrological meanings of the parameters expressed by Manning's equation to obtain a data set containing the elevations of the river beds throughout the basin. The second advancement is the provision of parameter uncertainties and, therefore, the uncertainties in the rated discharge. The third advancement concerns estimating the discharge while considering backwater effects. We analyzed the Amazon Basin using nearly one thousand series that were obtained from ENVISAT and Jason-2 altimetry for more than 100 tributaries. Discharge values and related uncertainties were obtained from the rain-discharge MGB-IPH model. We used a global optimization algorithm based on the Monte Carlo Markov Chain and Bayesian framework to determine the rating curves. The data were randomly allocated into 80% calibration and 20% validation subsets. A comparison with the validation samples produced a Nash-Sutcliffe efficiency ($E_{ns}$) of 0.68. When the MGB discharge uncertainties were less than 5%, the $E_{ns}$ value increased to 0.81 (mean). A comparison with the in situ discharge resulted in an $E_{ns}$ value of 0.71 for the validation samples (and 0.77 for calibration). The $E_{ns}$ values at the mouths of the rivers that experienced backwater effects significantly improved when the mean monthly slope was included in the RC. Our RCs were not mission-dependent, and the $E_{ns}$ value was preserved when applying ENVISAT rating curves to Jason-2 altimetry at crossovers. The cease-to-flow parameter of our RCs provided a good proxy for determining river bed elevation. This proxy was validated against Acoustic Doppler current profiler (ADCP) cross sections with an accuracy of more than 90%. Altimetry measurements are routinely delivered within a few days, and this RC data set provides a simple and cost-effective tool for predicting discharge throughout the basin in nearly real time.

## 1. Introduction

The number of gauging stations is decreasing worldwide [*Vörösmarty et al.*, 2000], which is causing an increasing reliance on satellite altimetry to provide information regarding inland waters. Hydrologists have adapted (and continue to adapt) new tools for improving knowledge and understanding continental scale fluxes to increase the global coverage of discharge monitoring. Discharge measurements are costly and time consuming, and available discharge data are generally obtained from locally calculated rating curves (RCs) that are based on a small number of simultaneous stage and discharge measurements. Discharge data are rarely distributed with uncertainty, although this value is generally calculated using a RC, which has its own uncertainty. Previous altimetric missions, such as Topex/Poséidon, ERS2 and ENVISAT, and current altimetric missions (Jason-2 and SARAL) are useful for monitoring continental water levels. According to *Bjerklie et al.* [2003], discharge can be estimated only from remotely sensed data sources, such as the slope, width and depth of medium to large rivers [*Dingman and Bjerklie*, 2005; *Birkinshauw et al.*, 2014]. Water depths and upstream in situ discharge can be merged to estimate the discharge at ungauged sites [*Birkinshaw*

*et al.*, 2010; *Tarpanelli et al.*, 2013]. Recent studies have proposed using inverse methods based on Manning's equation to estimate the discharge from remotely sensed observations of water surface elevation, width, and slope [*Durand et al.*, 2014; *Garambois and Monnier*, 2015]. *Gleason et al.* [2015] indicated that useful discharge estimates can be retrieved for some types of river reaches from satellite estimates of the river width and the log-linear relationships of at-a-station hydraulic geometries (AHG) [*Gleason and Smith*, 2014]. The pioneering work of *Jasinski et al.* [2001] produced discharge estimates based on Topex/Poséidon data over the Amazon by comparing altimetric water heights with gauge measurements, which demonstrated the feasibility of deducing river discharge from remote sensing data and in situ data. This and other studies conducted over the Ob' [*Kouraev et al.*, 2005], Amazon [*Zakharova et al.*, 2006], Gange [*Papa et al.*, 2010], Zambezi [*Michailovsky et al.*, 2012], and Mekong Rivers [*Birkinshaw et al.*, 2014] have estimated river discharge using remote sensing data. However, quality assessment has always relied on the location of a gauging station with (often) unknown accuracy. *Leon et al.* [2006] and *Getirana et al.* [2009] were the first to combine a rainfall-runoff model with RCs for estimating river discharge from radar altimetry. In addition, *Getirana and Peters-Lidard* [2013] were the first to compile a large data set of RCs spread across the entire Amazon Basin. The altimetry data set used in *Getirana and Peters-Lidard* [2013] is a subset of the data set used in this study. *Leon et al.* [2006] also showed that the physical characteristics of river reaches may be deduced from RC parameters. However, these physical characteristics were not preserved in other works, such as those of *Getirana and Peters-Lidard* [2013], *Finsen et al.* [2014], and *Dubey et al.* [2015].

Recently, RC uncertainty has been studied. For example, studies by *Clarke* [1999], *Herschy* [1999], and *Clarke et al.* [2000] were based on the residual variance of the power law regression between the in situ and rated discharge. *Petersen-Overleir and Reitan* [2005] included the possible heteroscedasticity of RCs for stage-discharge fitting (including multisegment RCs, floodplain representation, and hysteresis). These authors showed that the classic nonlinear least squares method may not consider heteroscedasticity and unphysical parameters. Markov Chain Monte-Carlo (MCMC) and Bayesian inference are satisfactory methods for addressing the uncertainty of output parameters, and the efficiencies of these methods have been proven in several studies. *McMillan et al.* [2010] studied the uncertainty of river flow using a single segment RC over a gravel-bed river in New Zealand. *Durand et al.* [2014] used water surface elevation and in situ slope measurements to evaluate the discharge, effective roughness coefficient and river bathymetry using a Bayesian MCMC scheme for a 11 km reach of the Severn River (UK). *Moyeed and Clarke* [2005] showed that Bayesian methods are effective for calculating RCs using case studies of small and large watersheds with drainage areas ranging from 6000 to $4.6 \times 10^6$ km². However, some limitations were detected, such as the calculation of the hydraulic exponents.

Recent developments in the post processing of satellite altimetry data have produced accurate data for the Amazon Basin [*Santos da Silva et al.*, 2010]. Vast amount of information regarding water levels have been collected at high spatial resolutions over the past decade and is organized in virtual stations (VS). A VS is defined by the location where the groundtrack of a satellite orbit crosses the reach of a river. During the past few years, the use of radar altimetry for inland waters has been investigated by the scientific community [*Birkett et al.* [2002], *Calmant and Seyler* [2006], *Alsdorf et al.* [2007], *Calmant et al.* [2008], among others]. According to *Santos da Silva et al.* [2010], ENVISAT altimetric data are suitable for rivers and typically exhibit errors of 0.12–0.40 m.

In this study, we demonstrate the feasibility of determining a physically consistent RC data set from radar altimetry and simulated discharges from the entire Amazon Basin. The quality of the RCs is quantified through their parameters and based on how the rated discharges (i.e., discharges that are calculated through the RCs) fit the simulated and in situ data. A sensitivity analysis for Cal/Val data sets and parameter ranges is performed, and sources of error are investigated.

## 2. Rating Curve and Stage-Discharge Relationship

RCs represent the hydraulic behavior of a channel section or reach and are a mathematical representation of stage-discharge relationships that can be defined by hydrologists using gauge data and empirical knowledge. To fit the actual behavior of the studied reach of the river, the user must obtain information regarding the large variety of hydrological conditions between extreme discharge and stage values. *Potter and Walker* [1985] have argued that obtaining reliable stage or discharge data under extreme conditions can be

difficult. However, this difficulty may be overcome using remote sensing techniques, which provide information for all flow conditions. Previous hydrological studies [*Lambie*, 1978; *Rantz et al.*, 1982; *ISO* 1100-2, 1998] have shown that this relationship should take the following form:

$$Q(t) = a \times h(t)^b, \tag{1}$$

where $Q(t)$ stands for the discharge at the river reach cross section at time $t$, $h(t)$ stands for the water depth at time t, and $a$ and $b$ are constant parameters in the equation. The term $h(t)$ can be written as $h(t) = (H(t) - Z_0)$, where $H(t)$ is the elevation of the water surface, whether measured by satellites or at a gauge; and $Z_0$ stands for the river bed elevation. This equation results in the following RC equation:

$$Q(t) = a \times (H(t) - Z_0)^b. \tag{2}$$

Under steady and uniform flow conditions, Manning's equation [*Manning*, 1891] is given as follows (3):

$$Q = n^{-1} A R^{2/3} S^{1/2}, \tag{3}$$

where $R$ is the hydraulic radius, $A$ is the cross section area, $n$ is Manning's roughness coefficient, and $S$ is the slope of the hydraulic gradient line. For large rivers (where the width is more than 10 times greater than the depth) with a rectangular section, equation (3) can be rewritten as follows:

$$Q = n^{-1} B S^{1/2} h^{5/3}, \tag{4}$$

where $B$ stands for the water surface width of the river reach. Next, the RC parameters can be related in equation (1) using Manning's equation to obtain $a = n^{-1} B S^{1/2}$. The coefficients $a$, $b$, and $Z_0$ from equation (2) are unique for each channel reach and depend on its physical characteristics, with $a$ as an indicator of channel geometry, roughness, and type of control and $b$ as an indicator of the geometry of the section at various depths [*Rantz et al.*, 1982]. Although the theoretical values of these parameters can easily be determined for artificial channels, these parameters are harder to determine for natural irregular shapes. *Bjerklie et al.* [2003] developed a set of statistical regressions that were based on equation (1) to estimate discharge when not all elements can be observed. Because the parameters of RCs are obtained by fitting discharge and stage data, they may not assume the exact values given by Manning's equation but should approximate these values. In fact, parameters that are grouped into $a$ may vary with the flow conditions and, consequently, vary with the stage. These variations result in a $b$ value that is slightly different from the theoretical value of 5/3. Thus, $a$ stands for the mean value of the hydrological parameters that may vary during the hydrological cycle. The most likely minimum and maximum values for each parameter can be estimated. Setting feasible parameter values is an important step because badly defined values can result in biased or overly constrained RCs. Consequently, we chose to establish a wide range of meaningful values for the three parameters, namely, $a$, $b$, and $Z_0$, as explained in section 3.3.

The common method used to obtain $a$, $b$, and $Z_0$ values is to fit the stage and discharge pairs using the linearized form of equation (2), which is given by $Ln(Q) = Ln(a) + bLn(H - Z_o)$ [*Leon et al.*, 2006; *Getirana and Peters-Lidard*, 2013]. Only the $a$ and $b$ parameters can be fit in this way. In latter studies, $Z_0$ was determined empirically as the value that minimizes the cost function of the least-square fit of $a$ and $b$. However, *Getirana and Peters-Lidard* [2013] showed that this method often leads to results that do not converge, (e.g., when the best fit is obtained for $Z_0 = \infty$) or that converge only at meaningless values. *Birkinshaw et al.* [2010] assumed that the mean flow velocities are equal in the upstream and downstream reaches of a given section [*Moramarco and Singh*, 2001; *Moramarco et al.*, 2005] to obtain a quadratic stage-discharge relationship (in this case, $b$ is forced and equals 2). Recently, *Dubey et al.* [2015] proposed using the minimum value in the water height series. However, this method forces null discharge at the height selected for $Z_0$.

The aforementioned methods do not provide an easy method for evaluating parameter uncertainties. One alternative to estimating the three RC parameters with their uncertainty is to use global optimization techniques that are coupled with the Bayesian inference scheme, as described below.

The determination of the RC of a river section is directly related to the assumption that the analytical relationship between the stage and discharge is univocal, i.e., only one possible discharge value can exist for a stage measurement. This assumption is valid for rivers with stable bed geometry and invariable downstream control. However, some reaches can exhibit high nonunivocity, resulting in heteroscedastic stage/
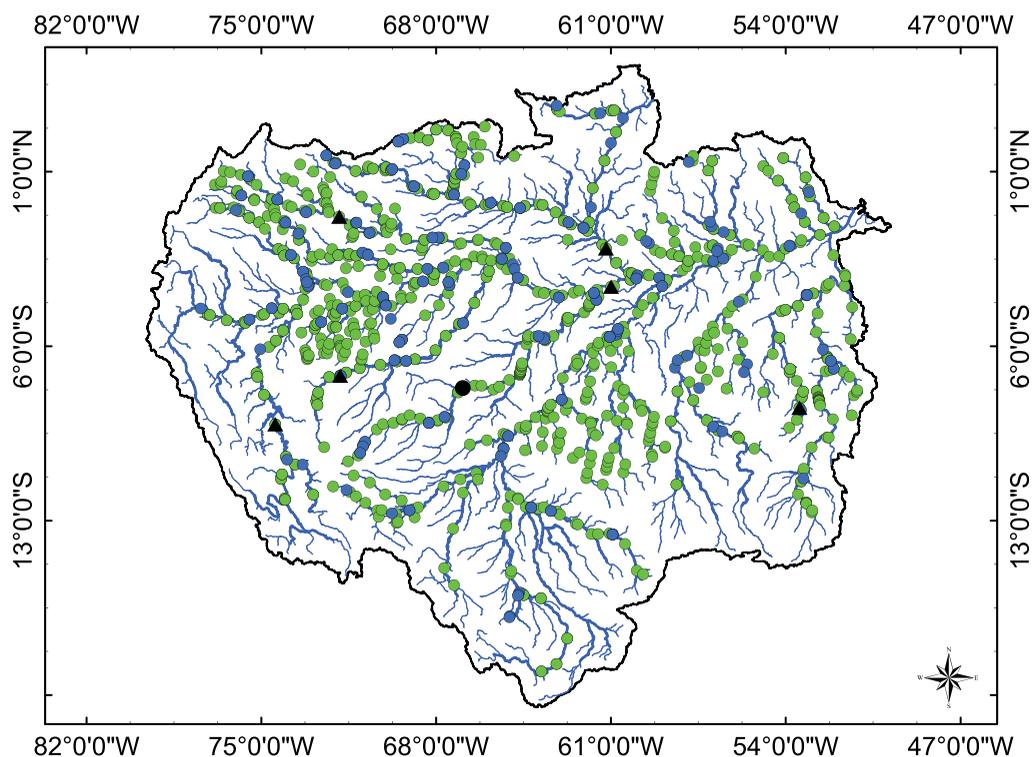
**Figure 1.** Locations of the 920 virtual stations of this study across the Amazon basin. The main river streams are shown as blue lines, and the limits of the Amazon basin are shown by black lines. ENVISAT virtual stations are indicated by green circles, and the Jason-2 virtual stations are indicated by blue circles. The six virtual stations are represented by black triangles, and the intersection of the ENVISAT groundtrack 908 with the Purus River is shown by a black circle.

discharge pairs when the downstream control varies. Therefore, the source of this variability must be investigated to ensure that the variability is related to data input error rather than a nonunivocal stage/discharge relationship. When nonunivocity is detected, the form of the RCs can be rewritten to include the slope as a variable parameter according to Manning's equation. This approach is discussed in section 4.4.

## 3. Materials and Methods

We propose a method for curve fitting based on satellite altimetry and model discharge estimates. Discharge estimates for the Amazon Basin were obtained from the fully validated MGB-IPH Amazon Basin model using a 1-D hydrodynamic representation [*Paiva et al.*, 2011, 2013a, 2013c], and discharge data were assimilated using Ensemble Kalman Filters (EnKF) at the stream gauges [*Paiva et al.*, 2013b] (see below). We used the Shuffled Complex Evolution Metropolis [*Vrugt et al.*, 2003] global optimization algorithm, which is based on the MCMC method and Bayesian inference scheme (as described below), to optimize the curve parameters and determine the confidence intervals for the estimated discharge and parameters. The surface water elevation at 920 virtual stations (with locations throughout the entire basin) was used to evaluate the performance of the optimization algorithm (see Figure 1). The VSs are derived from the ENVISAT (711 VS) and Jason-2 (209 VS) space altimetry missions. As shown in Figure 1, the VSs are spread throughout the basin and are located on the major tributaries and on much smaller reaches. These VSs are used to monitor more than a hundred rivers, which range in size from ten to thousands of meters in width and exhibit mean annual discharges of less than 100 m$^3$/s to more than 200,000 m$^3$/s.

### 3.1. MGB-IPH Hydrodynamic Model

In this section, we describe the method developed by *Paiva et al.* [2013a] for estimation discharge and associated uncertainty methods that are relevant to our study. These methods include hydrological simulation and RC-interpolated discharge assimilation, as described in the above section. The MGB-IPH model [*Collischonn*

*et al.*, 2007] is a distributed large-scale process-based hydrological model coupled with a hydrodynamic module that uses a storage model for floodplains [*Paiva et al.*, 2011]. In the MGB-IPH model, the entire Amazon Basin is divided into 5765 elementary catchments. The components used to generate the flow into each catchment include the soil water budget (bucket model), energy budget, evapotranspiration (Penman Monteith), and surface, subsurface and groundwater flow. Next, the generated flow is routed to the stream using a linear reservoir model, and the river flow is routed using the Muskingum-Cunge method or hydrodynamic modeling. The hydrodynamic model solves the full 1-D Saint Venant's equations and represents flooded areas as simple storage areas. The information needed to represent the river channel hydrodynamics was extracted from the Digital Elevation Model, which was obtained by the Shuttle Radar Topography Mission (SRTM) [*Farr et al.*, 2007]. Parameters such as river width and depth were calculated as a function of drainage area using the geomorphological equations developed at the stream gauging stations [*Paiva et al.*, 2013a].

Assimilation of the gauge data was performed using the rated discharge and EnKF technique *Paiva et al.* [2013b] showed that the EnKF performed well for assimilating in situ discharge and was a valuable method for improving model estimates in gauged and ungauged river reaches. This improvement in performance was propagated to ungauged locations through hydrodynamics.

*Paiva et al.* [2013b] evaluated the discharge uncertainties at each miniature basin based on comparisons of the gauging stations and error estimations of rainfall rates. The relative error for the discharge estimation was determined using a normally distributed discharge function. The model output is a set of the discharges and discharge uncertainties for each catchment, which are used as inputs in our global optimization scheme.

### 3.2. Altimetry Data

The altimetric data set used in this study was created by *Santos da Silva et al.* [2010, 2012, 2014]. This data set consists of more than 1000 VSs that provide a water height time series over the Amazon Basin. In addition, these series mainly result from the ENVISAT and Jason-2 missions. At some locations, the water height time series was obtained from older missions, such as ERS2 or Topex/Poséidon. The basinwide distribution of this data set can be used to obtain water elevation time series for main and second-order rivers. In this study, we examined 920 VSs that were located over the central low declivity area, the northern and southern shields, and the Andes piedmont (see Figure 1 for location). The span for the altimetric series was from 2002 to 2010 for ENVISAT and from 2008 to 2012 for Jason-2. We did not consider the ERS-2 and Topex-Poséidon series because of their lower qualities. *Frappart et al.* [2006] reported that good quality time series over continental water bodies can be obtained through the ICE1 retracking of the raw radar echoes procedure, which has not been applied to the ERS2 and T/P missions yet. ENVISAT provides repeat measurements every 35 days, with a height accuracy of a few tens of centimeters. Jason-2 has similar accuracy, with measurements obtained every 10 days. These repetition cycles provided nearly 80 and 70 stage/discharge pairs, respectively. Details regarding altimetry data processing and quality assessment can be found in *Santos da Silva et al.* [2010]. We split the data into two subpopulations, one for the calibration of the RCs and the other for validation. As explained later in this paper, tests were conducted to determine which information should be removed from the series to perform validation without calibration errors. Gaussian noise was added to the observation to include the time series error, which was approximately 35 cm for ENVISAT [*Santos da Silva et al.*, 2010], as follows:

$$H_{in} = H_{altim} + N(0, \ \sigma^2), \tag{5}$$

where $H_{in}$ (m) is the height input in the method, $H_{altim}$ is the original height, $\sigma$ is 0.35 m, and $N$ is the normal distribution function. The water height estimates by ENVISAT and Jason-2 that were used in this study are referenced in EGM2008 [*Pavlis et al.*, 2012] and were corrected for systematic bias using the bias values published by *Calmant et al.* [2012] for ENVISAT and by *Seyler et al.* [2013] for Jason-2.

Many of our results are illustrated using VS at the intersection of the Purus River and groundtrack 908 of the ENVISAT mission, hereafter called SF-Purus-ENV-908. This particular VS was selected because of its corresponding proximity to the Seringal Fortaleza in situ gauging station and because Purus is an intermediate sized tributary of the Amazon River (see Figure 1 for localization). The above characteristics make this VS representative of the basin and provide a sufficiently high quantity of data for evaluations from simulated and gauge data.

### 3.3. Global Optimization Method

One of the biggest issues in RC optimization methods is the evaluation of parameter uncertainty while considering various error sources (errors for stage values and discharge estimates, simplification of physical reality, mathematical model formulation). The SCEM-UA (Shuffled Complex Evolution Metropolis) [*Vrugt et al.*, 2003] global optimization algorithm is based on the Markov Chain Monte Carlo method and Bayesian framework. A Markov chain is a mathematical system without memory in which a new state depends on only the preceding state. Although deterministic methodologies [*Leon et al.*, 2006; *Getirana et al.*, 2009] provide either a unique solution for RC optimization or no solution, the stochastic MCMC method provides an ensemble of possible parameter values within a user-defined parameter space, the density distribution of these parameters, and confidence intervals for the discharge estimates. Furthermore, this method provides a best estimate that corresponds to the discharge estimates with the lowest error relative to the input. Bayesian methods for fitting RCs have been explored by *Moyeed and Clarke* [2005]. These authors concluded that MCMC optimization techniques are efficient for determining the posterior uncertainty limits over discharge parameters and estimates.

The optimization algorithm chosen used the quadratic error of the discharges as the objective function to classify the solutions for the evolution of the populationas follows:

$$\varepsilon = \sum \left( Q_r(t) - Q_o(t) \right)^2, \tag{6}$$

where $Q_r(t)$ represents the rated discharge (flow from applying the RC equation) and $Q_o(t)$ is the reference discharge at the same time. In our case, the reference discharge is the MGB prediction. As explained above, Gaussian noise was added to the model discharge and water elevation observations before sampling. Standard deviation values were obtained from the error that was associated with each daily discharge estimate from MGB-IPH and from the usually accepted RMS value of 0.35 m for the discharge and height, respectively.

A posterior probability function (the probability of a parameter given the observed data, e.g., the model discharge) is provided by the Bayesian inference method for each optimized parameter based on the user-defined prior distribution. The initial population is built according to predefined extreme values and a priori distributions and then split into complexes that are tuned using parallel Markov chains until they reach convergence conditions and/or the maximum number of iterations, as explained below. The algorithm output consists of the posterior distribution for each optimization parameter, which is used to predict the uncertainty boundaries of the model simulations. We followed the method of *Vrugt et al.* [2003], who recommended using a population (*s*) of 100 individuals and 5 complexes (*q*) in reasonably simple optimization problems. An example of an initial population and its evolution after each iteration is presented in Figure 2. To build this figure, we used SF-Purus-ENV-908 and limited the algorithm to 2500 iterations. Figure 2 includes random drawings of each individual sequence in the set of feasible parameters and the evolution of the population towards a stationary distribution (identified by the higher density of dots in a specific area of the parameter set).

The convergence of the MCMC sampler is assessed using the Gelman and Rubin criterion, which is a scale reduction (SR) factor. *Gelman and Rubin* [1992] developed a method for determining whether a solution was converging with the stationary posterior distribution to decrease the processing time of the convergence assessment. The SR factor can be calculated as follows:

$$\sqrt{SR} = \sqrt{\frac{g-1}{g} + \frac{q+1}{n}\frac{B}{W}}, \tag{7}$$

where $g$ is the number of iterations within each sequence, $n$ is the total number of draws, $B$ is the variance between the means of the $q$ sequence, and $W$ is the mean variance between the Markov chains. *Gelman and Rubin* [1992] proposed a limit of 1.2 for declaring convergence because it is difficult to achieve a score of 1. Additional algorithm information regarding the strategies used for the evolution or classification of sequences can be found in *Vrugt et al.* [2003]. The SR factor was described by *Gelman and Rubin* [1992] and evaluates whether the independent Markov chains, starting from random points, converge to the same distribution by comparing the interchain and intrachain variance. An illustration of the SR factor for typical VSs can be seen in Figure 3, where the factor for each parameter has been drawn using up to 5000 iterations.
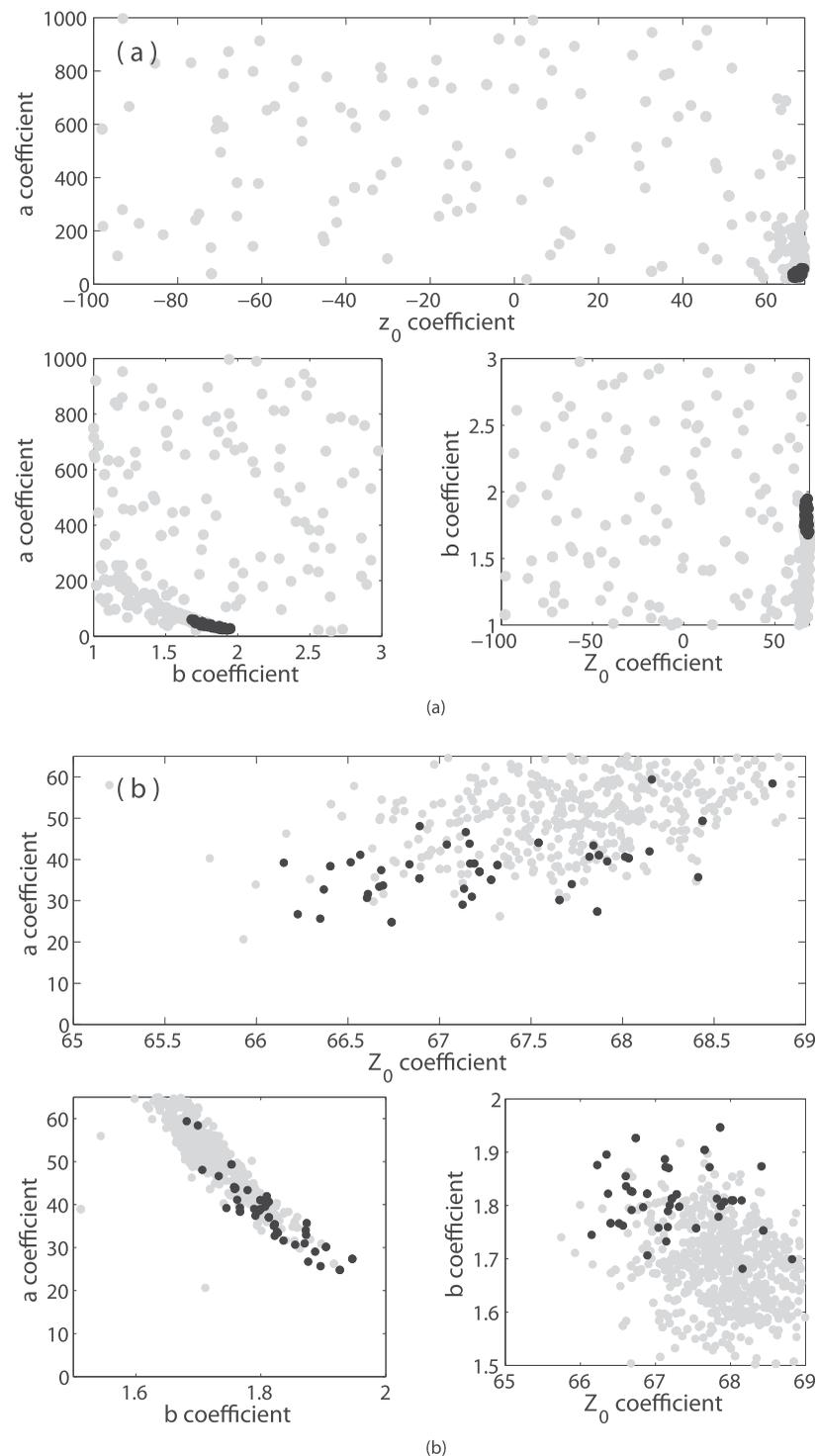
**Figure 2.** Scatter plot showing the evolution of the populations of the parameter sets *a*, *b*, and $Z_0$ in the entire range of possible values (a) and in a restricted range for better visualization (b). The gray dots are the populations from 1 to 2499 iterations, and the black dots are the populations after 2500 iterations. The upper half is the *a* parameter against the $Z_0$ parameter. The lower left section is the *a* parameter against the *b* parameter, and the lower right section is the *b* parameter against the $Z_0$ parameter.

Figure 3 demonstrates that the algorithm requires approximately 1000–2000 iterations for the parallel sequences to converge to a stationary posterior distribution. In addition, the differences between the last SR evaluations were calculated and compared to a predefined break value, which determined whether the algorithm would stop or continue. We set the break value at $1 \times 10^{-3}$, as suggested by *Vrugt et al.* [2003].

**Figure 3.** Scale reduction factors (SRs) of each of the virtual stations for the first 5000 iterations: (a) Iriri River VSs, (b) Jurua River VSs, (c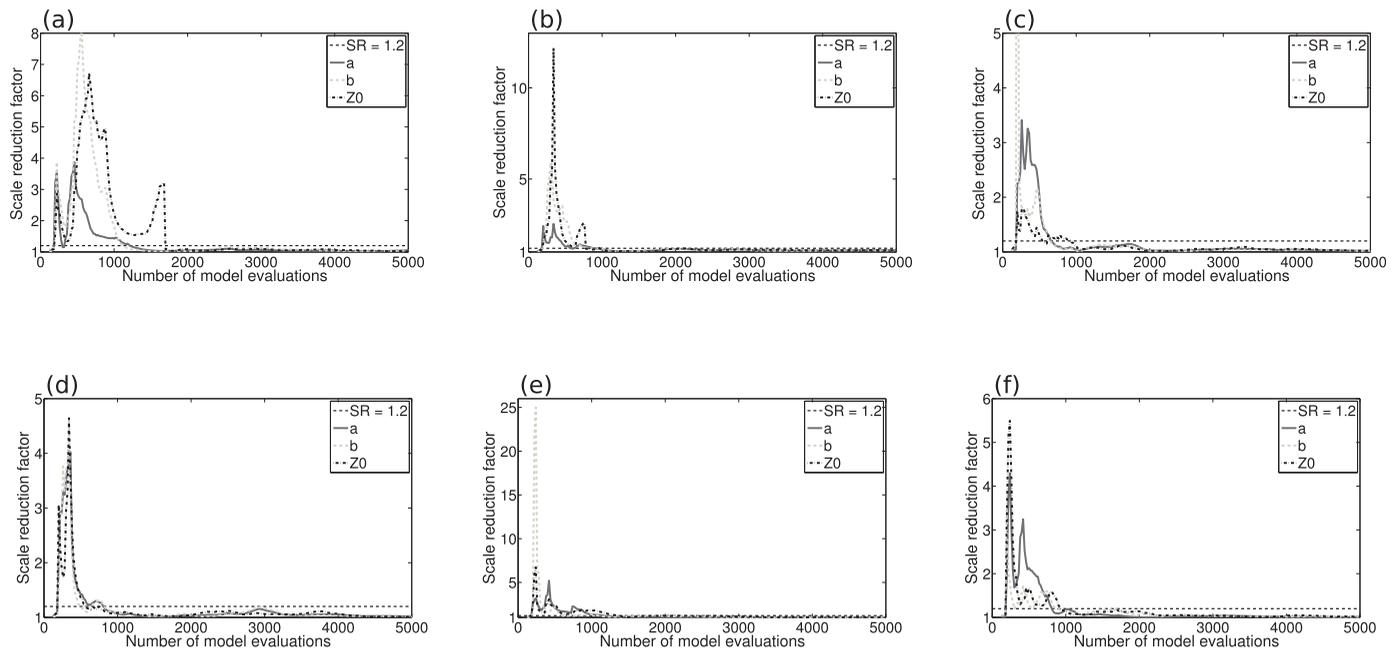) Ucayali River VSs, (d) Solimões River VSs, (e) Japura River VSs, and (f) Negro River VSs. The continuous gray line is the SR for the *a* parameter, the dashed gray line is the SR of the "b" parameter, and the dashed black line is the SR for the $Z_0$ parameter.

An evaluation of the algorithm efficiency should include verifying the physical consistency of the optimized parameters. For example, *Chow et al*. [1988] demonstrated that the value of *b* should vary from 1.3 for wide rivers to more than 2 for relatively narrow rivers. Therefore, we chose a range of acceptable values between 1 and 3 to loosen the constraints of the *b* parameter. The possible range of values for the "*a*" parameter is from 0 to 1000. Although *b* is supposed to represent the channel geometry, the *a* and *b* coefficients could be related between sections, as noted by *Gleason and Smith* [2014]. This relationship between the values of *a* and *b* along rivers is used for external parameter validation.

Theoretically, the range of $Z_0$ values is easier to determine for a reach with a rectangular cross section. This coefficient represents the cease-to-flow elevation and can be approximated by measuring the elevation of the river bed at the station. At any time, the elevation of the river bed equals the elevation of the free surface minus the water depth. However, this measurement is difficult to achieve in deep natural channels or channels with an irregular shape. The range of possible values is determined by assuming that the cease-to-flow height for each studied location must be lower than the smallest elevation in the time series and that the mean depth must be less than 100 m. The mean depth of 100 m was chosen because it is a largely acceptable assumption for Amazonian rivers. Within this ranges, each parameter can vary with the same probability, i.e., the a priori Probability Density Function (PDF) of each parameter is a constant. Furthermore, the algorithm allows one to indicate an informative a priori PDF, such as when an acceptable first guess is known for one parameter. In this case, the PDF is noninformative because the available information was already used to build the ranges. We tested the sensitivity of our method to the initial ranges of the parameters, which were consistent with the alternate analytical formulation of RCs proposed by *Dingman and Sharma* [1997].

### 3.4. Performance Coefficients

We evaluated the performance of our procedure using two classical hydrological indicators, the Nash-Sutcliffe efficiency ($E_{ns}$) [*Nash and Sutcliffe*, 1970] indicator and the normalized root mean square error (*NRMSE*) indicator. As explained above, our RCs were developed from "observed" discharges (i.e., discharges that were issued from the simulation and perturbed within their uncertainty). The RC performance was evaluated against these reference discharges and the available in situ data. This approach is explained in section 4.3. $E_{ns}$ is frequently used for evaluating hydrological models. This value is comparable to the mean quadratic error with the variance of the observed series and can vary from $-\infty$ to 1, with $-\infty$ being the worst

**Table 1.** Coordinates of the Six Virtual Stations and the Mean Values of the MGB Discharges for Each Station

| River | Margin | Latitude (°) | Longitude (°) | Mean Discharge (m³/s) |
|---|---|---|---|---|
| Iriri | Right | −8.47 | −53.45 | 440 |
| Jurua | Right | −7.18 | −17.85 | 1,100 |
| Ucayali | Main | −9.13 | −74.44 | 6,250 |
| Solimões | Main | −3.61 | −61.00 | 100,300 |
| Japura | Left | −0.80 | −71.88 | 6,300 |
| Negro | Left | −2.07 | −61.21 | 31,800 |

result and 1 indicating perfect equality between the observed and rated discharges. A value of 0 indicates that using the rated discharge is equivalent to using the mean of the input series. Furthermore, $E_{ns}$ can be calculated as follows:

$$E_{ns} = 1 - \frac{\sum \left( Q_r(t) - Q_o(t) \right)^2}{\sum \left( Q_o(t) - \overline{Q_o(t)} \right)^2}, \quad (8)$$

where $\overline{Q_o(t)}$ is the mean of the reference discharge series. The other performance coefficient used to evaluate the RC efficiency is the *NRMSE*, which is calculated as follows:

$$NRMSE = 100 \; \frac{\sqrt{\frac{\sum \left( Q_r(t) - Q_o(t) \right)^2}{n}}}{Q_{min} - Q_{max}}, \quad (9)$$

where $Q_{min}$ and $Q_{max}$ are the maximum and minimum discharges in the observed series, respectively. The coefficients were estimated using three different configurations. First, $E_{ns}$ and *NRMSE* were estimated comparing the altimetry-based rated discharges with the model discharges at each VS for the calibration subpopulation. Second, the performance coefficients were calculated at the same locations using the validation subpopulation (VS validation), which consists of independent data from the data used for RC fitting. Finally, a third evaluation (Gauge validation) was performed with gauging stations where possible. We calculated $E_{ns}$ and *NRMSE* for all three experiments and evaluated the consistency of the RC parameters in terms of the river geometry. When the seasonal variability is large relative to the variability at other time scales, $E_{ns}$ and *NRMSE* mainly indicate the quality of fit for the seasonal variability. Therefore, we estimated the impacts of seasonality on the quality of the RCs by computing $E_{ns}$ in two ways. First, $E_{ns}$ was calculated between the monthly means of the MGB-IPH and rated discharges, whose performance is hereafter referred to as $E_{ns-clim}$. Second, $E_{ns}$ was calculated using the residuals between the actual values and the corresponding monthly mean. The latter performance is referred to as $E_{ns-resid}$. In addition to the fit of the rated discharges with the in situ and MGB-IPH discharges, we investigated the reliabilities of the estimated coefficients (considering their physical meanings) and the consistencies of the parameter uncertainties (considering the ranges and sizes of the credibility intervals).

Throughout this paper, we present examples of results obtained from using our method for the 6 VSs, whose locations are highlighted in Figure 1. These VSs were chosen because they are representative of the basin and our results and provide adequate sampling of the left and right margins and the latitude and longitude ranges of the basin. In addition, these VSs provide a sample of the large range of mean discharges, which varies between O (100) m³/s and O (100.10³) m³/s, in the basin. Table 1 presents the coordinates and mean discharges of these six VSs.

## 4. Results

Following the methods presented in section 3, we evaluate the fit between the height observations and simulated discharge. The MGB model discharge data are assumed accurate and are used to calculate the algorithm's objective function because in situ discharge data are not available at the required spatial and temporal resolutions. This optimization process ensures the best quantification of the RCs' accuracy. Because satellite height observations are representative of a river's dynamics, the rating developments should smooth any model simulation errors. The time window for the model that was run and that of the altimetry series are not the same. Therefore, the calibration and validation procedure was conducted during the overlapping period (2002–2009 for ENVISAT VS and 2008–2009 for Jason-2 VS).

### 4.1. Calibration and Validation Subpopulations

The first step of this study was to determine the number of (H-Q) pairs to use for calibration and validation. The ENVISAT and Jason-2 missions provided approximately 70 measurements over the temporal span of

**Table 2.** Size of the 95% Confidence Intervals for Each Experiment (Lines) and the Selected Virtual Stations (columns) at High and Low Flows

| Withdrawn data | VS1 | | VS2 | | VS3 | | VS4 | | VS5 | | VS6 | |
|---|---|---|---|---|---|---|---|---|---|---|---|---|
| | Low Q | High Q | Low Q | High Q | Low Q | High Q | Low Q | High Q | Low Q | High Q | Low Q | High Q |
| 0% (ref.) | ±84% | ±38% | ±54% | ±42% | ±69% | ±30% | ±45% | ±31% | ±14% | ±10% | ±81% | ±33% |
| 10% | ±98% | ±41% | ±54% | ±42% | ±61% | ±39% | ±48% | ±34% | ±15% | ±13% | ±88% | ±30% |
| 20% | ±145% | ±45% | ±57% | ±45% | ±69% | ±38% | ±52% | ±36% | ±17% | ±14% | ±76% | ±32% |
| 30% | ±194% | ±37% | ±61% | ±49% | ±76% | ±36% | ±50% | ±34% | ±16% | ±12% | ±103% | ±31% |
| 40% | ±130% | ±43% | ±62% | ±49% | ±52% | ±31% | ±49% | ±35% | ±19% | ±16% | ±63% | ±35% |
| 50% | ±187% | ±47% | ±78% | ±56% | ±91% | ±41% | ±56% | ±40% | ±20% | ±17% | ±113% | ±33% |

the study for each VS during the considered time frame. We determined the optimal amount of data for use in the calibration period and for determining limits to achieve good calibration. This step was considered necessary because of critical event occurrences during the temporal coverage of the series. For example, extreme flood or drought events could be ignored if one period was used for calibration and a different period was used for validation, which would affect the curve fitting results. For this test, we used the VSs shown in Figure 1. We performed the entire optimization process for the complete series (71 stage measurements) for each VS and randomly removed 10–50% of the points (in 10% increments) from the original series.

As expected, the uncertainty of the rated discharge increased when the number of pairs used for calibration decreased, as shown in Table 2. The smallest confidence intervals were observed when the entire series was used or only 10–20% of the series was used. The 95% confidence interval ranged from ±14% (entire series) to ±20% (50% of pairs withdrawn) at low discharges and from ±10% (entire series) to ±17% (50% of pairs withdrawn) at high discharges for the VSs that presented the best results. The uncertainty of the discharge was higher when 30–40% of the pairs were withdrawn. The ranges for the lower and higher discharges slightly improved when 50% of the pairs were withdrawn. This behavior was expected because fitting a scatter plot with fewer stage/discharge pairs results in a tighter confidence interval. Optimization parameters must be considered to determine how much input data can be withdrawn from the original series without affecting the optimization results.

The parameters that were obtained from the optimization algorithm when considering the entire series were chosen as reference parameters to evaluate the errors that resulted from withdrawing data. The parameters from successive trials were compared with those from each VS. The average uncertainty was determined from the error obtained from evaluating the coefficients, as shown in Table 3. Withdrawal of 10% and 20% resulted in the best estimation of the parameters, and withdrawal of 30%, 40%, and 50% resulted in the worst estimations for the three coefficients.

The results in Tables 2 and 3 prompted us to calibrate the optimization process using 80% of the data from the series. The remaining 20% of data was used for validation.

### 4.2. Optimization Results and Parameter Estimates

In this section, we present optimization process values for the "$a$", "$b$," and "$Z_0$" coefficients and the sensitivity analysis results. The global correlation between the stage and discharge for the six selected VSs is shown in Figure 4.

**Table 3.** Differences in the Optimal Values of the $a$, $b$, and $Z_0$ Coefficients From the Optimization of the Entire Series for Each Experiment and for the Six Virtual Stations

| Withdrawn Data | Coefficient | | |
|---|---|---|---|
| | a | b | $Z_0$ |
| 10% | ±12.5% | ±2.5% | ±1.5% |
| 20% | ±13% | ±3% | ±0.5% |
| 30% | ±15% | ±2.5% | ±2% |
| 40% | ±27% | ±6.5% | ±2.5% |
| 50% | ±142.5% | ±6% | ±2.5% |

First, we present the results in terms of RC fitting and evaluate the "$a$", "$b$," and "$Z_0$" parameters. The algorithm converged before the maximum number of iterations. The results for the "$a$" and "$b$" coefficients (Figure 5) are consistent with the assumptions from equation (4) (see explanations below) and with the expected values. The mean value of the "$a$" parameter for the ENVISAT VSs was 188, and the mean value of the "$b$" parameter was 1.67.
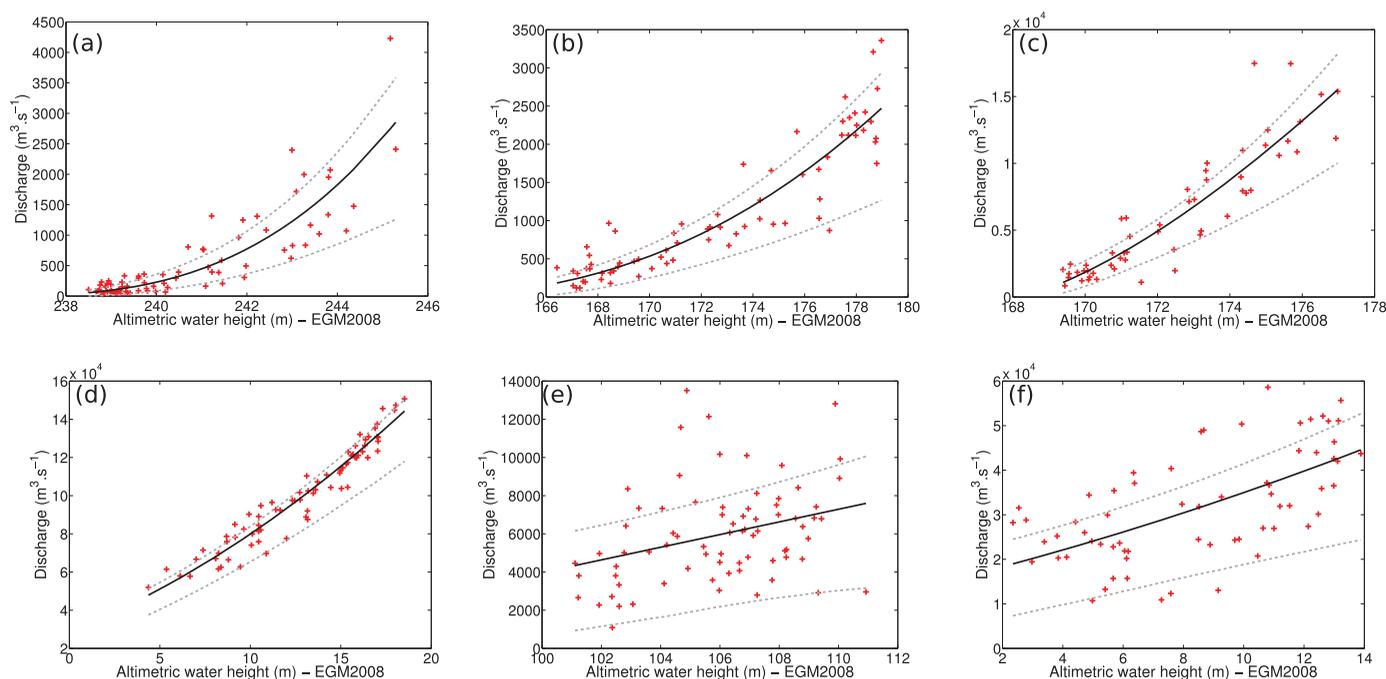
**Figure 4.** Stage/discharge relationships for the six virtual stations: (a) Iriri_592_03, (b) Jurua_708_02, (c) Ucayali_336_03, (d) Solimões_106_01, (e) Japura_794_01, and (f) Negro_693_01. The red crosses show the water elevations versus the MGB discharges pairs. The best fit RC is the black line, and the dashed gray lines represent the borders of the 95% confidence interval.

Half of the values for *a* were between 15 and 230, and half of the values for *b* were between 1.2 and 2, with less than 10% of the *b* values exceeding 2.5 (as shown in Table 4). Similar results were obtained for the Jason-2 VSs, with mean values of 1.69 for *b* and 221 for *a*. Half of the *a* values were within the interval of [26; 265], and half of the *b* values were within the interval of [1.15; 2.1]. According to equation (4), the values of *b* should be approximately 5/3 if the Manning-Strickler equation is respected. Differences with the theoretical value can be explained by the cross-section geometry and the departure of the flow regime from steady flow. The intervals that we found for *b* include the theoretical value of 5/3, indicating that the overall physical consistencies of the parameters are maintained, even when the fitting process is automatic. The few VSs with *a* or *b* coefficients near the current bounds have poor adjustment, e.g., low $E_{ns}$, which suggests that these stations may represent specific cases in which the RC equation must be defined more carefully. In this case, the main problems are the poor model discharge estimates obtained at these locations or the impossibility to apply the Manning's equation.

*Gleason and Wang* [2015] showed that the AMGH relationship established by *Gleason and Smith* [2014] could be supported between the a and b coefficient pairs along a river as long as a given discharge flows through the same area along the cross sections of the channel. We tested the existence of such a relationship between the (a, b) pairs along two different rivers, the Purus River and the Iriri River. The Purus River is more than 3000 km long, has a mean discharge of 11500 m$^3$/s, and is highly meandrous. The Iriri River is a braided affluent of the Xingu River that is approximately 1300 km long with a mean discharge at its mouth of 2900 m$^3$/s. We identified a trend between $\ln \frac{1}{a}$ and $\ln \frac{1}{b}$ to be consistent with the AMGH formulation. Figure 6 shows that this trend is clear for the Purus River but less clear for the Iriri River. Consequently, we concluded that the (a, b) pairs found for the Purus River are sufficient for depicting the AMGH property where it exists.

The $Z_0$ parameter and the associated mean depth are presented in Figure 7. The mean depth was computed for each VS by calculating the mean elevation values in the altimetric series and subtracting the value of $Z_0$ from the optimization algorithm. The $Z_0$ values are referenced in the EGM 2008 geoid model as they are in the altimetry series. The $Z_0$ values throughout the basin (illustrated in Figure 7) are consistent with the expected values, with the lowest values observed in the central area of the basin and the highest values observed in the western and southwestern parts of the Andes piedmonts. The estimated $Z_0$ values ranged
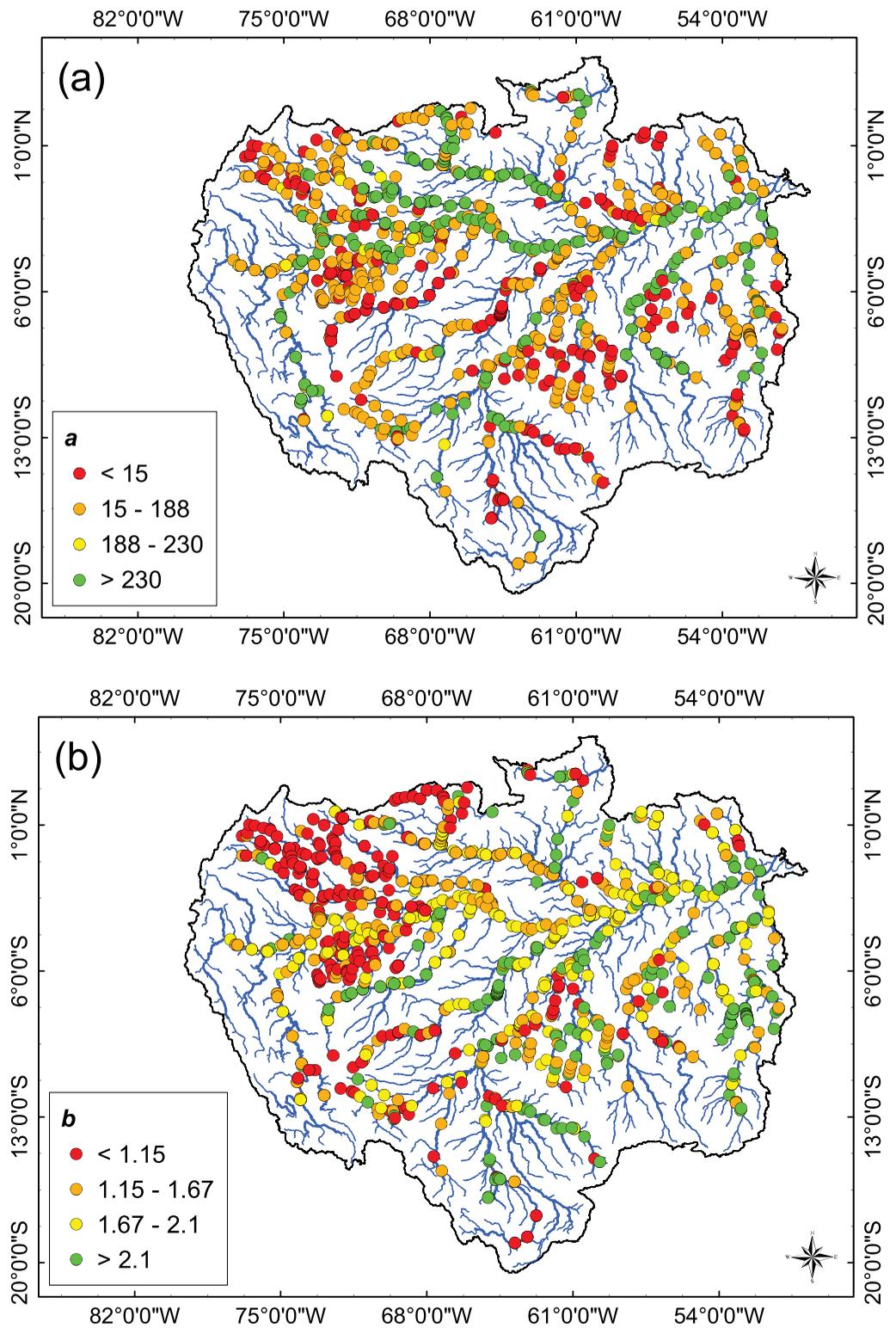
**Figure 5.** Spatial distribution of the *a* coefficient (a) and spatial distribution of the *b* coefficient (b) after the RC optimization process. The values are identified by different colors, with red corresponding to the lowest values, orange and yellow corresponding to intermediate values, and green corresponding to the highest values. The values range from zero to 1000 for *a* and from 1 to 3 for *b*, as explained in the text.

**Table 4.** Characteristic a and b Values for the ENVISAT and Jason-2 Virtual Stations, Including the Mean, 25% Percentile and 75% Percentile

|  | ENVISAT | | Jason-2 | |
|---|---|---|---|---|
|  | *a* | *b* | *a* | *b* |
| Mean | 188 | 1.67 | 221 | 1.69 |
| 25% percentile | 15 | 1.2 | 26 | 1.15 |
| 75% percentile | 230 | 2 | 265 | 2.1 |

from −33 m near the mouth to 560 m in the upper Grande River. Consequently, river depths of 10 m and less than 3 m were estimated in the central basin area and in the upper streams of most of the rivers, respectively. These results also show that the method converges to correctly evaluate the cease-to-flow elevation, resulting in reliable mean river depths.

We also tested the algorithm's sensitivity to the initial range of possible values for the *a*, *b*, and $Z_0$ parameters to determine whether the parameter estimates were strongly constrained by setting a realistic range of initial values. Table 5 illustrates the results of sensitivity tests for the three parameters in the case of SF-Purus-ENV-908 for four experiments. Each experiment relies on changes in *a*, *b*, or $Z_0$ for experiments one, two and three, respectively, and changes in all three parameters for the fourth experiment. The "Best RC"
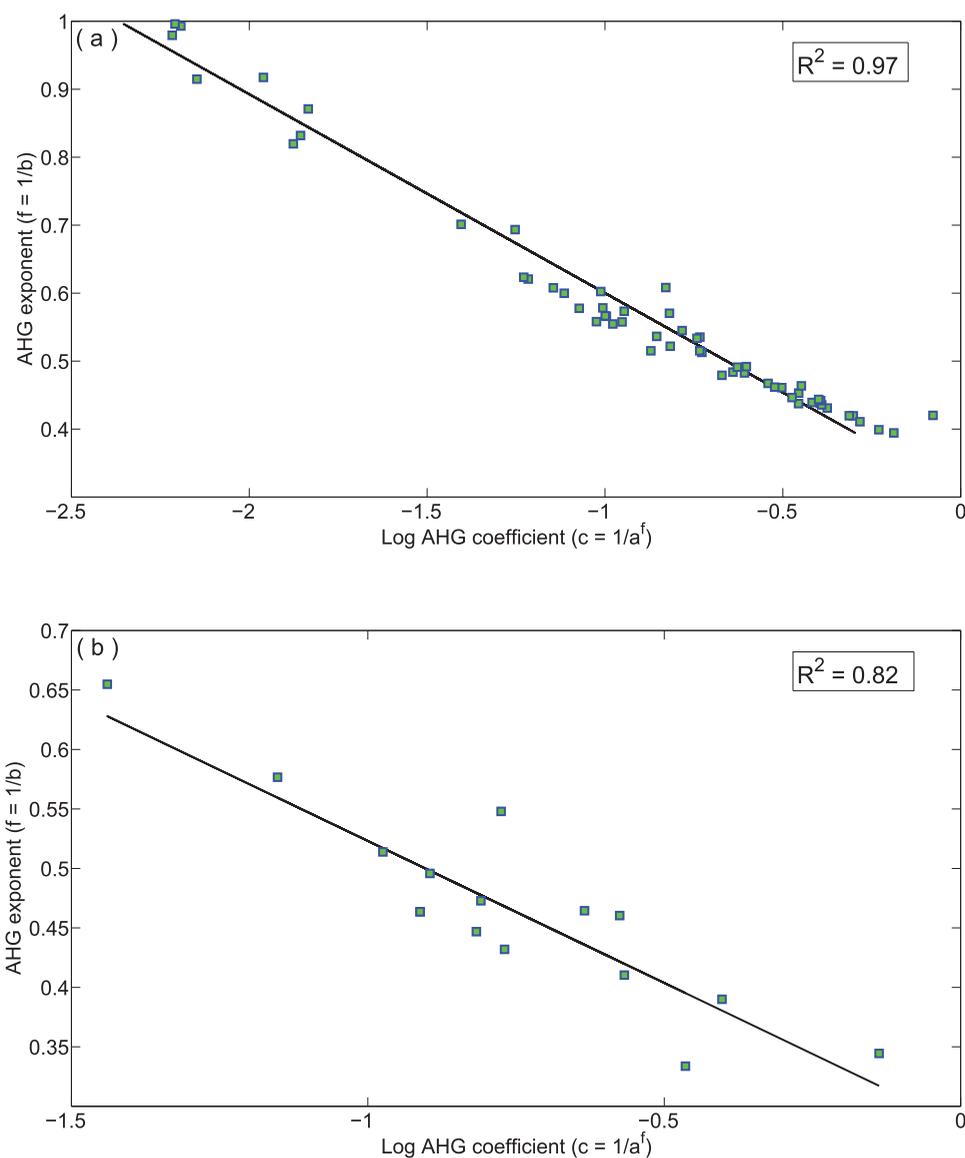


**Figure 6.** Relationships between the RC parameters "*a*" and "*b*," as expressed by *Gleason and Smith* [2014] for the Purus River (a) and Iriri River (b). The blue-filled dots are the coefficient values, and the black line is the linear interpolation of the scatter plot.
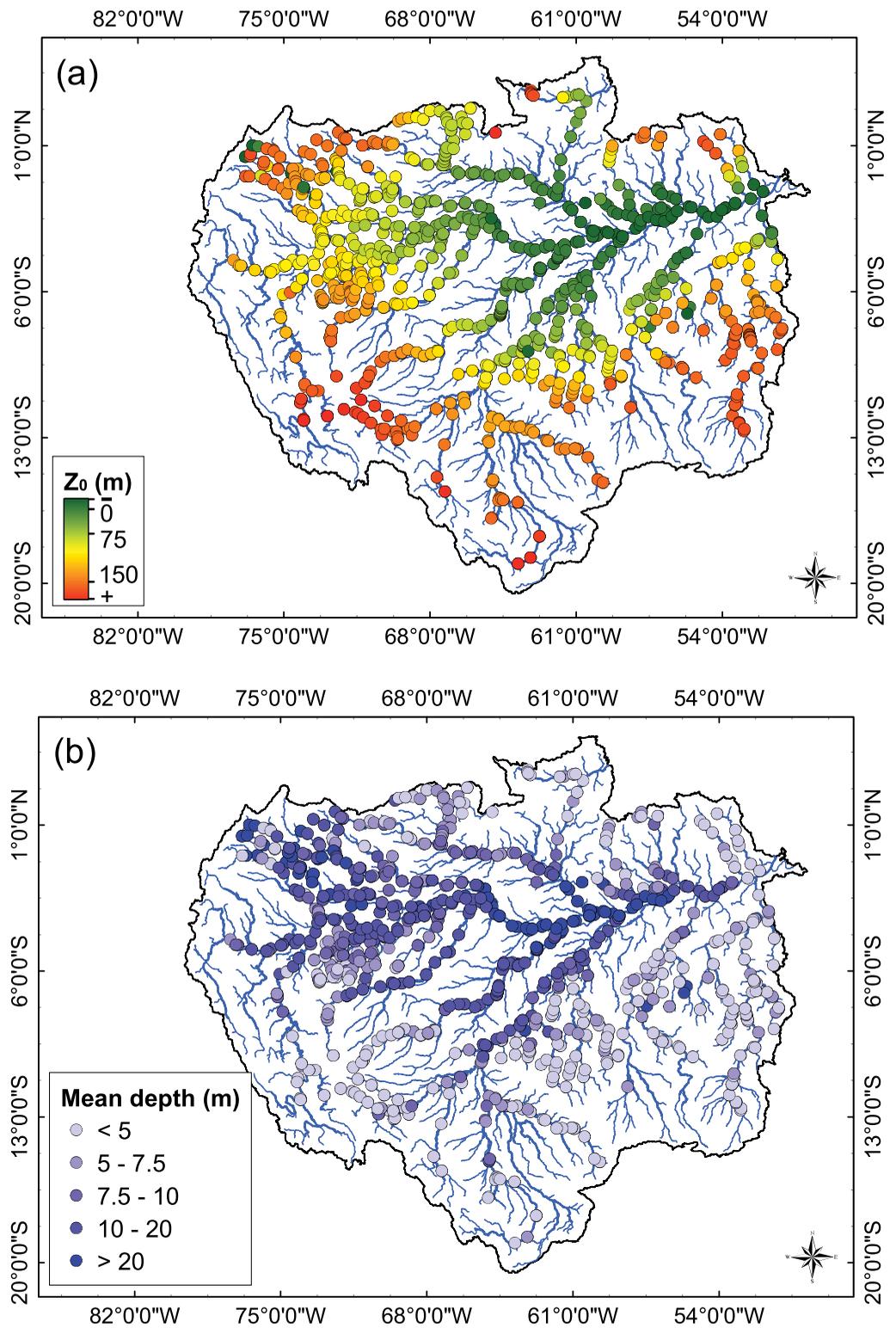
**Figure 7.** Cease-to-flow parameter (a) and the calculated mean water depth (b) in meters for the 920 virtual stations in this study. The mean depth was estimated from the mean altimetric height and the $Z_0$ parameters at each VS. Higher values of $Z_0$ are shown in red and lower values are shown in green. Higher mean depths are shown in dark blue and lower depths are shown in light blue.

**Table 5.** Values of the $a$, $b$, and $Z_0$ Parameters for the Different Initial Ranges and Associated Standard Deviations, $E_{NS}$ Score, and *NRMSE*

|  | Initial | | | First exp. | | | Second exp. | | | Third exp. | | | Fourth exp. | | |
|---|---|---|---|---|---|---|---|---|---|---|---|---|---|---|---|
|  | $a$ | $b$ | $Z_0$ | $a$ | $b$ | $Z_0$ | $a$ | $b$ | $Z_0$ | $a$ | $b$ | $Z_0$ | $a$ | $b$ | $Z_0$ |
| Best RC | 24.224 | 1.91 | 66.03 | 21.12 | 1.94 | 65.56 | 17.59 | 2.02 | 65.89 | 29.26 | 1.86 | 66.45 | 19.55 | 1.99 | 66.15 |
| Mode | 36.37 | 1.79 | 66.58 | 33.16 | 1.70 | 67.49 | 15.73 | 1.80 | 64.59 | 18.42 | 2.00 | 65.73 | 20.00 | 1.98 | 66.01 |
| Std | 23.49 | 0.12 | 0.92 | 18.50 | 0.10 | 0.82 | 24.19 | 0.12 | 0.88 | 25.74 | 0.12 | 0.84 | 13.30 | 0.10 | 0.79 |
| $E_{ns}$ |  | 0.92 |  |  | 0.93 |  |  | 0.93 |  |  | 0.92 |  |  | 0.94 |  |
| *NRMSE* |  | 9.14 |  |  | 8.80 |  |  | 8.88 |  |  | 9.38 |  |  | 8.63 |  |

line shows the results for the best parameter evaluation (the line that marks the RC). "Mode" represents the mode of each parameter, e.g., the most frequent value in the population, and "Std" represents the standard deviation of each parameter (e.g., dispersion from the average).

In the first experiment, the $a$ parameter varied over the interval of [0; 100,000], in the second experiment, the $b$ parameter varied over the interval of [0; 10], and in the third experiment, the $Z_0$ parameter varied over the interval of [$-1000$; $H_{min}-0.2$]. In the fourth experiment, the ranges of the three parameters varied together. In the initial experiment, intervals of [0; 1000], [1; 3] and [$-100$; $H_{min}-0.2$] were used for $a$, $b$, and $Z_0$, respectively. The standard deviations of the parameters (Table 5) indicated that changing the initial ranges of the parameters did not substantially affect the results in terms of $E_{ns}$ and *NRMSE* or the final parameters of the RC.

### 4.3. Discharge Estimates

We now consider whether the rated discharges are consistent with the reference discharges from either the MGB model or the gauging stations. The $E_{ns}$ and *NRMSE* values were calculated for the calibration and validation subpopulations for the entire set of VSs and are shown in Table 6. For the calibration subset, the median and mean values of $E_{ns}$ were 0.81 and 0.7, respectively, with 25% of the VSs showing $E_{ns}$ values greater than 0.91. For the validation subset, the median and mean values were 0.81 and 0.68, respectively, which are acceptable considering the spread of VSs across the basin and over a large range of river sizes. The worst $E_{ns}$ values were generally obtained for the upstream VSs. During calibration, 75% of the VSs had an $E_{ns}$ value that was higher than 0.57 (0.56 for validation) and an *NRMSE* value that was lower than 11.8% (12.7% for validation) (Table 6). The median *NRMSE* values were 8.9% for calibration and 9.9% for validation.

Good results were obtained for the main stream of the Amazon River and its major tributaries, as shown in Table 7. The mean $E_{ns}$ was higher than 0.9 in the Amazon, Madeira, and Solimões Rivers and higher than 0.75 in the Negro, Purus, Tapajós, and Xingu Rivers. Smaller reaches also had good $E_{ns}$ scores, which indicated good method performance for wide and narrow rivers. However, the results were not as good for the Colombian portion of the Japura-Caquetá River and the Putumayo-Içà River. Dense sampling of these basins is also available from altimetry, i.e., 80 VSs or approximately 9% of the data set. The bad results obtained in these basins affected the mean $E_{ns}$ and *NRMSE* values. Calculating the discharge from these two specific rivers is a significant issue, as suggested by *Paiva et al.* [2013b] and confirmed by our attempt to determine the RC. These results are supported by the MGB discharge and altimetry height pairs and the RCs for the VSs shown in Figure 4 and by the modeled and calculated hydrographs from the VSs shown in Figure 8.

The tributaries with a lower $E_{ns}$ shown in Table 7 had higher standard deviations, ranging from 4.8 to 6.5%, than the other tributaries, which had standard deviations ranging from 0.9 to 2.2%. For these tributaries, the slight degradation of $E_{ns}$ was not related to the river width. However, the $E_{ns}$ performance coefficient was correlated with large uncertainties in the discharge, as issued from the MGB. The results were generally worse at the VSs where the mean discharge uncertainty was higher than 10%, although some stations still exhibited good $E_{ns}$ and *NRMSE* values.

The $E_{ns}$ values between the calculated and modeled discharges are presented globally in Figure 9. Figure 9a provides the $E_{ns}$ at each VS

**Table 6.** Performance Coefficients ($E_{ns}$ and *NRMSE*) and Statistics for Calibration and Validation

|  | $E_{ns}$ | | *NRMSE* (%) | |
|---|---|---|---|---|
|  | Calib. | Valid. | Calib. | Valid. |
| Mean | 0.70 | 0.68 | 9.6 | 10.6 |
| 25% Percentile | 0.57 | 0.56 | 11.8 | 12.7 |
| Median | 0.81 | 0.81 | 8.9 | 9.9 |
| 75% Percentile | 0.91 | 0.91 | 6.7 | 7.0 |

**Table 7.** Cal/Val Performances ($E_{ns}$ and $NRMSE$) for Some of the Main Tributaries of the Amazon River in Sensitivity Analyses

|                  | $E_{ns}$ |        | $NRMSE$ (%) |        |
|------------------|----------|--------|-------------|--------|
|                  | Calib.   | Valid. | Calib.      | Valid. |
| Amazon           | 0.91     | 0.93   | 7.5         | 7.2    |
| Madeira          | 0.92     | 0.93   | 7.6         | 6.9    |
| Negro            | 0.75     | 0.68   | 10.1        | 11.7   |
| Purus            | 0.75     | 0.75   | 6.4         | 10.8   |
| Solimões         | 0.91     | 0.93   | 6.4         | 7.2    |
| Tapajós          | 0.77     | 0.75   | 11.0        | 12.4   |
| Xingu            | 0.80     | 0.70   | 9.0         | 10.2   |
| Japura Caqueta   | 0.16     | 0.12   | 17.2        | 19.0   |
| Iça - Putumayo   | 0.11     | 0.09   | 19.8        | 19.7   |

for the calibration subpopulation, Figure 9b provides the $E_{ns}$ for the mean monthly discharges, and Figure 9c presents the $E_{ns}$ values from the residuals (i.e., after removing the monthly means from the discharge series). As expected, the $E_{ns}$ values in Figure 9 indicate that the method is adequate for retrieving the seasonal and residual components of the discharge signal, principally for the major reaches. Minor reaches exhibit more heterogeneous performance, illustrating the variable importance of the residual components among the VSs.

We also fit the discharge estimated from the optimized RC with gauge data. This step is important for verifying that the results and performance coefficients are sufficient for simulated discharge and discharge obtained from gauging stations. Thus, we used data from 51 gauging stations from the Brazilian water agency ANA (data available on the agency's website www.ana.gov.br) with discharge information from 2002 to 2012 that was obtained by transforming the gauge readings into discharge using local RCs. Our own rated discharges were calculated using the RC method and satellite data. The resulting $E_{ns}$ and $NRMSE$ values are presented in Table 8. Gauge validation was performed for 37 VSs from the ENVISAT mission and 14 VSs from the Jason-2 mission.

As expected, the overall coefficient values indicated high performance, with mean $E_{ns}$ values of 0.83 and 0.86 for ENVISAT and Jason-2, respectively, and mean $NRMSE$ values of 9.55% and 8%, respectively.

Finally, we tested the dependency of the RC to the mission that was used in the (stage, discharge) pairs building process. For this test, we selected 5 crossovers between Jason-2 and ENVISAT that occur close to a gauge. RCs that were based on ENVISAT altimetry were applied to the Jason-2 altimetry series for the 2010–2012 period, and the J2 rated discharges were compared with the gauge-rated discharges. In four of the five cases, $E_{ns}$ was higher than 0.5. The initial $E_{ns}$ values at these stations were all greater than 0.7, which suggests very
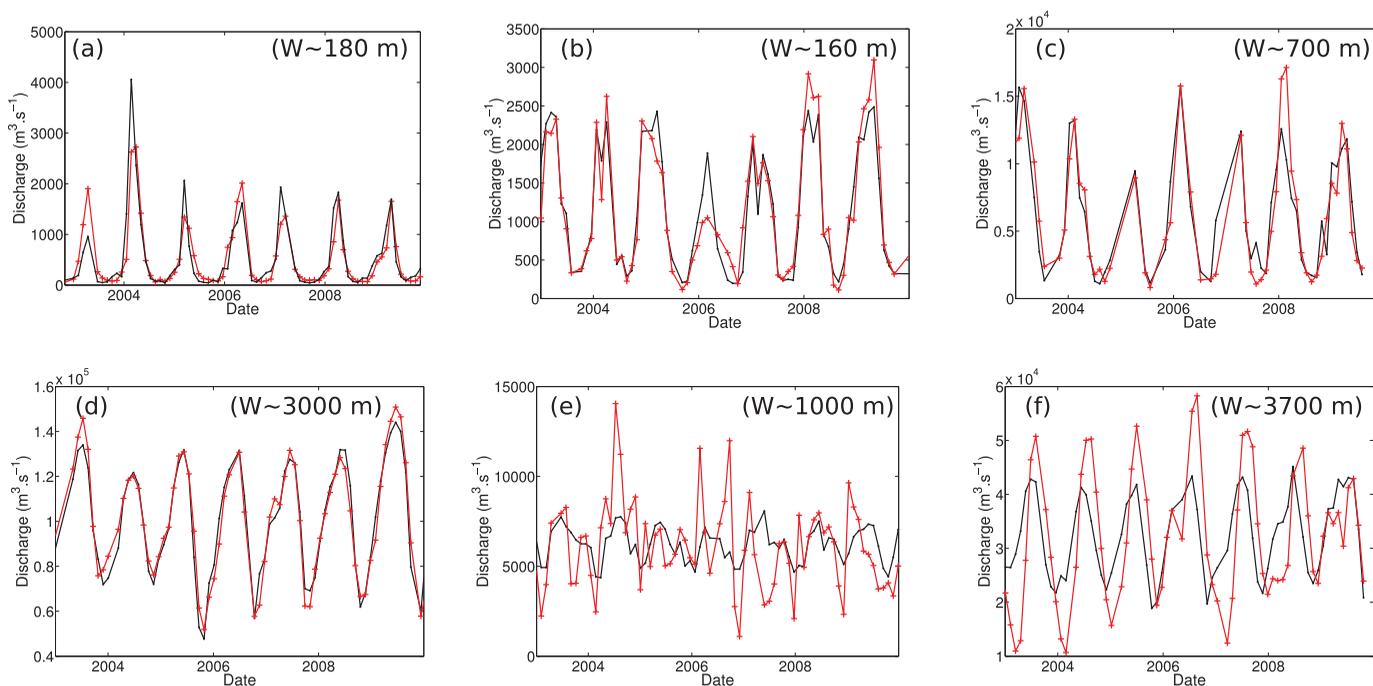


**Figure 8.** Hydrographs for the six virtual stations in Figure 1: (a) Iriri_592_03, (b) Jurua_708_02, (c) Ucayali_336_03, (d) Solimões_106_01, (e) Japura_794_01, and (f) Negro_693_01. The MGB discharges at dates with altimetric data are represented by the red line, and the rated discharges from altimetric data and rating curves are represented by the black line.
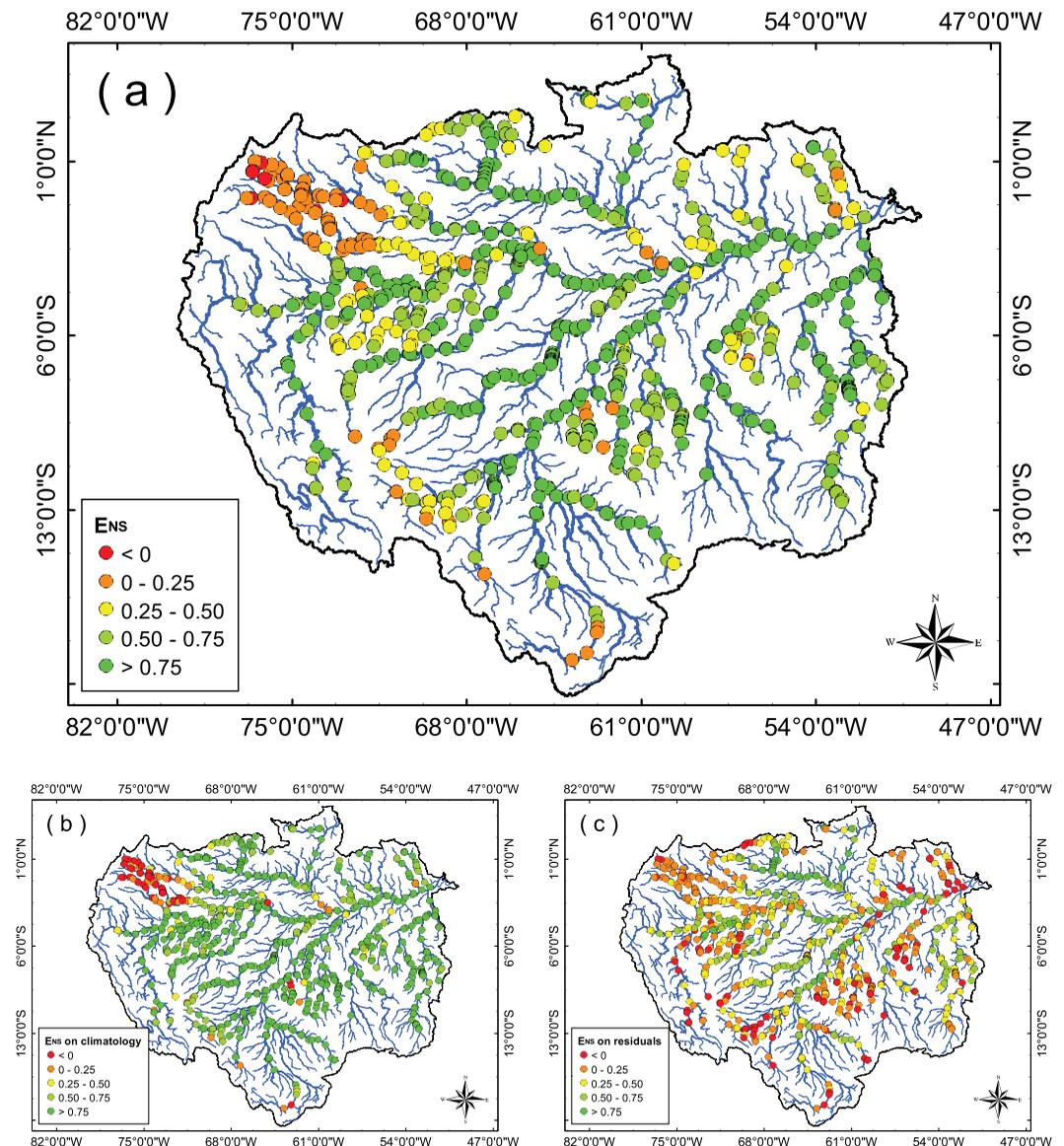
**Figure 9.** Climatological analysis of discharges estimates with (a) the full data set, (b) the climatological data, and (c) the residuals. The quality in terms of $E_{ns}$ is shown using a color scale, with red representing the worst values and green representing the best values.

limited degradation in the quality of the predictions. Conversely, low $E_{ns}$ values were observed for the VSs where the initial $E_{ns}$ value was already low (0.31). This result shows that the RC parameters from the ENVISAT data can be used to estimate the discharge from other altimetry missions, such as Jason-2. In addition, the stability of the $E_{ns}$ values with independent altimetry series can be used for identification when low $E_{ns}$ values likely occur because of problems encountered in the discharge series or the mathematical formulation used to define the RC (rather than in the altimetry series and as shown in the previous test). This point is discussed in section 4.4, paragraph 3.

### 4.4. Uncertainty Analysis

To demonstrate our method, we present the uncertainty analysis for the VS SF-Purus-ENV-908. The RC of this VS is presented in Figure 10a. The 95% confidence interval from the
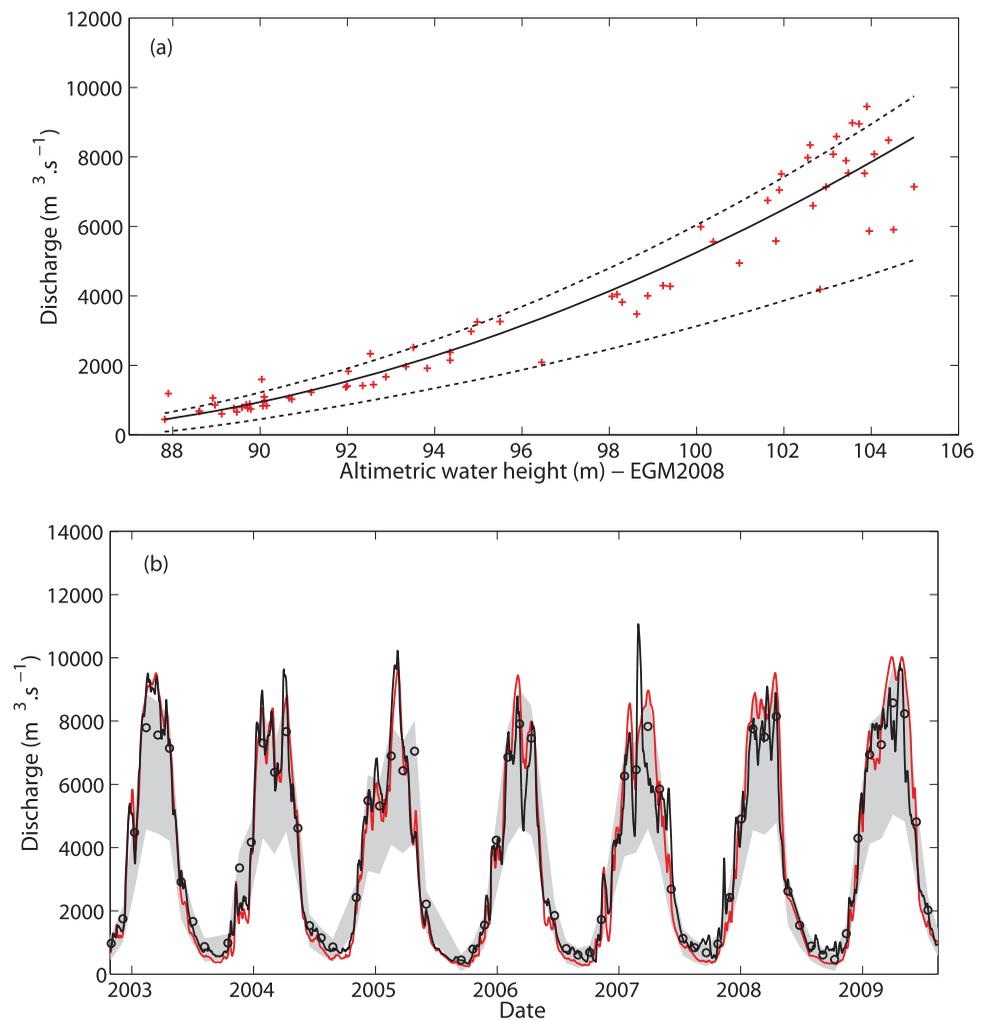
**Table 8.** Performance Coefficients ($E_{ns}$ and NRMSE) for the Validation Subsets of 37 ENVISAT SV and 14 J2 VS Near the 51 Gauging Stations

|  | $E_{ns}$ | | NRMSE (%) | |
|---|---|---|---|---|
|  | J2 | ENV | J2 | ENV |
| Mean | 0.86 | 0.83 | 8.04 | 9.55 |
| 25% percentile | 0.85 | 0.76 | 8.11 | 12.9 |
| Median | 0.92 | 0.91 | 7.70 | 6.93 |
| 75% percentile | 0.94 | 0.95 | 5.75 | 5.92 |

**Figure 10.** Rating curve (a) and hydrograph (b) for SV SF-Purus-ENV-908. (a) contains the MGB discharge/altimetric height pairs that are used as inputs for the rating curve calculation (red crosses) with the best fit rating curve (black continuous line) and the 95% confidence interval (dashed line), which was obtained after the optimization process. (b) displays the corresponding hydrograph and shows the in situ discharge from Seringal Fortaleza provided by ANA (red line), the MGB discharge (black line), and the rated discharge (dots) along with their associated 95% confidence intervals (gray).

PDFs of the RC parameters is also presented in Figures 10a and 10b. The first result is that nearly all of the in situ discharge measurements are within the confidence interval, which shows that the interval is meaningful. However, the range of possible discharge values for a given height measurement is quite large, indicating that the uncertainty in the reference discharges or RC parameters is large.

The observed hydrograph (provided by the ANA website) of Seringal Fortaleza is presented in Figure 10b with the MGB discharge, rated discharge, and 95% confidence interval. As apparent from the RC (Figure 10a), the range of the confidence interval is much larger for high flows than for low flows. This problem is inherent to the RC formulation. Indeed, according to equation (1), the uncertainty in the discharge $\sigma_Q$ can be expressed as follows:

$$\sigma_Q = b \, \frac{Q}{H} \, \sigma_H. \tag{10}$$

Because b >1, the uncertainty in the discharge $\sigma_Q$ for a given uncertainty in the water depth $\sigma_H$ is larger at high elevation than at low elevation and discharge.

The information used to perform RC optimization has three potential sources of error: bad discharge estimates, which mainly occur because of low quality input data sets; highly scattered altimetry data;

and the nonexistence of a single RC. When the discharge and stage are known with acceptable uncertainty, the source of discrepancies between the calculated and modeled discharge may result from the mathematical formulation that was chosen for the RC. Indeed, the backwater effect occurs in some cases of low declivity or in confluence areas [*Meade et al.*, 1991]. The backwater effect can result from physical obstructions to water flow or from the time lag between the peak discharge of the affluent and main stream. This effect can significantly change the free surface slope and plays an important role in extreme events, such as droughts [*Tomasella et al.*, 2010]. In agreement with Manning's equation, we account for slope variations to represent the heteroscedasticity of the relationship between the stage and discharge in these areas. One example of this approach is a VS near the confluence area of the Negro and Amazon Rivers, an area that is renowned as a paradigm of the backwater effect and where discharge measurements are regularly performed. The optimization of a classic single segment RC (experiment 1) leads to a poorly adjusted relationship ($E_{ns} = 0.202$). The same optimization process was repeated by including the water surface slope that was extracted from the two nearest VSs (one upstream and one downstream). The original relationship between the discharge and stage can be transformed as follows:

$$Q(t) = a.S(t)^c \times (H(t) - Z_0)^b, \tag{11}$$

where $S(t)$ is the free surface slope at the considered VS with time. This slope can be calculated in two different ways, by either performing separate calculations for each measurement date by temporally interpolating the upstream and downstream water height or by calculating a mean monthly slope from the entire data set. Interpolation was mandatory because the height measurements were not collected on the same dates in the three series. Performing tests with the two methods allowed us to choose the monthly mean value because the results were better than the results of the methods with daily interpolated values. According to equation (10), the exponent of the slope $c$ should be equal to 0.5; however, the real value may differ slightly from this theoretical value. Consequently, we conducted two additional experiments. In experiment 2, the slope exponent was fixed at 0.5, and in experiment 3, the exponent was allowed to vary with $a$, $b$ and $Z_0$.

We selected the VS at the mouth of the Negro River to show the capability of our method for providing a reliable discharge series in the context of a strong backwater effect. The optimization process improved the $E_{ns}$ by 130% (i.e., from 0.238 to 0.548) relative to experiment 1 (i.e., where the slope was considered constant) when $c$ was fixed at 0.5. The optimization process improved the $E_{ns}$ by 208% (i.e., from 0.238 to 0.73) when $c$ was let free to vary. The optimized value of $c$ was 0.367, which was similar to the value of 1/3 that was used in the Dingman-Sharma and Adjusted Prandtl-von Karman relationships [*Dingman and Sharma*, 1997]. The changes in the discharge estimates between the experiments are presented in Figure 11. The stage discharge pairs from experiments 1 and 3 are shown in Figure 12. Although the slope calculation (with mean monthly values) can still be improved, experiment 3 shows that good RCs can be achieved even in the presence of pronounced hysteresis and that low $E_{ns}$ values can be used to potentially identify reaches where the stage discharge relationship is not univocal and where temporal variations in the slope should be considered to determine the RC parameters. In addition to improving the $E_{ns}$ efficiency coefficient (identified by the improved fit between the rated and MGB hydrographs in Figure 11), the confidence interval significantly decreased between the experiments (from ±24% and ±23% for lower and higher discharges to ±20% and ±15%, respectively). Comparing the rated discharge with Acoustic Doppler current profiler (ADCP) measurements, which are also reported in Figure 11, confirmed that our results are reliable. From this example, we show that the backwater effect impacts the hydrological regimes of rivers with low declivity or confluences through slope variation and that this temporal variation must be considered during RC formulation.

## 5. Discussion

An in-depth critical analysis of our results shows that the methodology we used to obtain RCs over the Amazon Basin was adequate, with a mean $E_{ns}$ of 0.70 and a mean *NRMSE* of 9.6%. Splitting the series into monthly mean and residual climatology series showed that the climate of the discharge throughout the basin is depicted well by the rated discharge, with $E_{ns} > 0.5$ for nearly all of the VSs, except for the Içá and Japura VSs and for the VSs at the river mouths that experience backwater
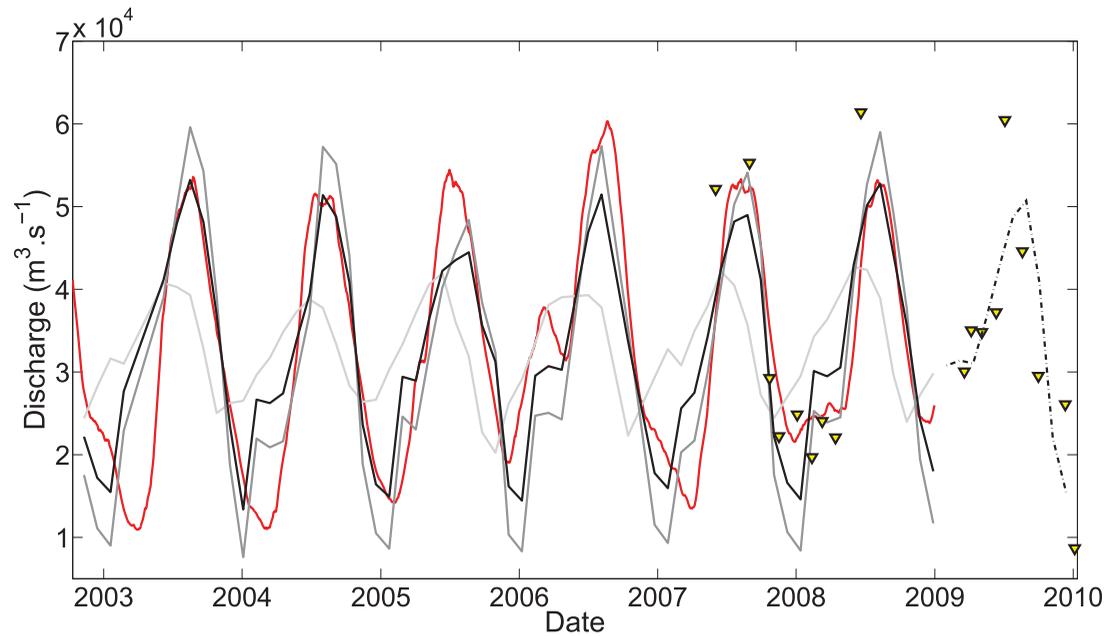
**Figure 11.** Hydrograph from a crossing of ENVISAT pass 106 and the Negro River near Paricatuba. The MGB discharges are shown by a red line, the rated discharges from experiment 1 (without considering the slope) are shown in light gray, the rated discharges for experiment 2 (slope included with the exponent fixed at 0.5) are shown in dark gray and the rated discharges for experiment 3 (slope included with a variable exponent) are shown in black. The ADCP measurements at Paricatuba are represented by yellow triangles, and the rated discharges for 2009 and 2010 from the ENVISAT heights are represented by black broken lines.

effects. Regarding the residuals, high $E_{ns}$ values were also found along all of the major contributors, including the Negro, Madeira, and Purus Rivers. Conversely, low $E_{ns}$ values were observed for the higher-order tributaries.
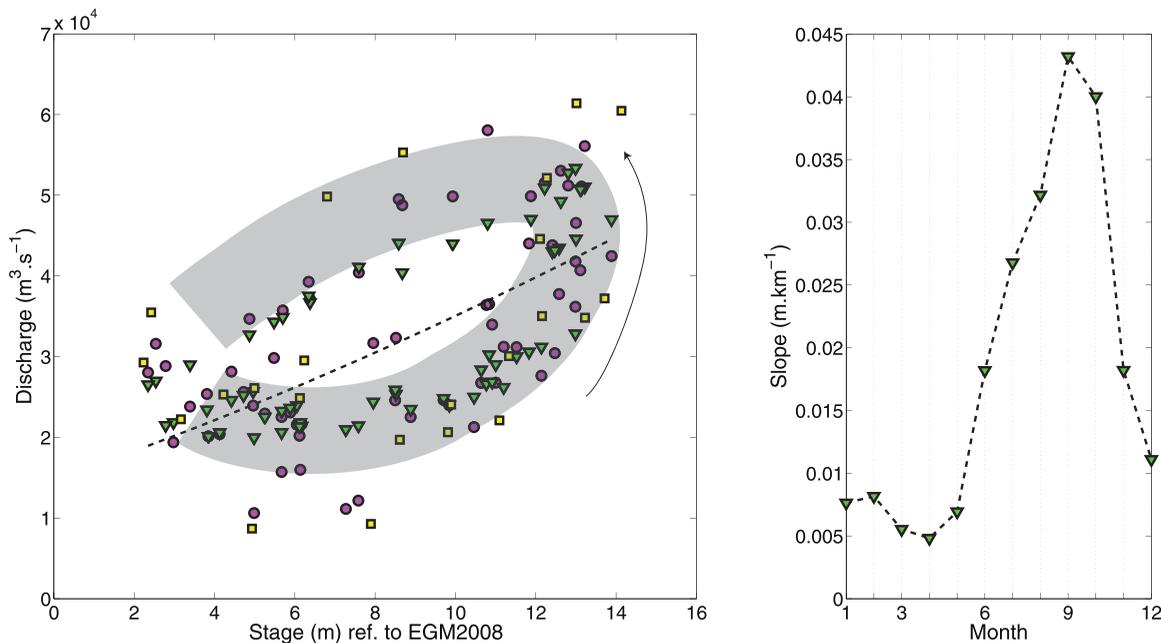


**Figure 12.** Rating curve calibration based on the temporal variability of the slope. (left half) scatter plot that shows (1) the MGB discharge and altimetric height pairs in purple circles; (2) the pairs that were obtained after optimization when not considering the slope variability in the rating curve equation shown as black broken lines (experiment 1); (3) the pairs that were obtained when considering the monthly slope shown as green triangles (experiment 3); and (4) the ADCP measurements at Paricatuba shown in yellow squares. This arrow provides a sense of the hydrological cycle. (right half) The mean monthly slope calculated from the ENVISAT heights from 2002 to 2009. The slope during low water was nearly 10 times smaller than the slope during high water.

**Table 9.** Validation of the $Z_0$ Coefficient Based on ADCP Measurements[a]

| Name | Latitude | Longitude | Month | Year | Distance (km) | AWD (m) | EWD (m) | Δ (%) |
|---|---|---|---|---|---|---|---|---|
| Foz Purus | −3.73 | −61.56 | September | 2010 | <1 | 19.29 | 20.27 | −5.1 |
| Itapeua | −4.029 | −62.997 | May | 2010 | 10 | 32.54 | 32.30 | <1 |
| Manacapuru | 3.326 | −60.553 | February | 2010 | 35 | 25.29 | 26.59 | −5.2 |
| Foz Madeira | −3.411 | −58.786 | December | 2009 | 6 | 9.25 | 9.78 | 5.8 |
| Itacoatiara | −3.17 | −58.409 | January | 2010 | >50 | 32.70 | 36.56 | −11.8 |
| Paricatuba | −3.069 | −60.263 | December | 2009 | <1 | 27.08 | 26.87 | <1 |
| Beruri | −3.911 | −61.394 | April | 2010 | 15 | 20.65 | 19.50 | 5.5 |

[a]AWD stands for the *water depth* that was derived from the ADCP measurements across the section; EWD stands for the *estimated water depth* and was obtained from the $Z_0$ parameter and altimetric water height; and Δ stands for the difference between AWD and EWD represented as the percent of AWD. The presented date is the date of the ADCP measurements. The latitude and longitude are the mean values between the left and right margins of the ADCP measurements.

These results represent a significant improvement relative to previous studies. The performance indices, such as $E_{ns}$ and *NRMSE*, are comparable with the performance indices of similar studies [*Getirana and Peters-Lidard*, 2013, *Finsen et al.*, 2014]. More specifically, the $E_{ns}$ values are slightly inferior to the values from *Getirana and Peters-Lidard* [2013] for the calibration period and are nearly equal for the validation period when considering the direct insertion experiment and are similar to the values reported by *Finsen et al.* [2014]. However, these studies focused on obtaining the best fits for discharge estimates and did not aim to preserve the physical significance of the RC parameters, as noted for the other aforementioned studies. Moreover, our study is the first study based on a large, multimission, altimetric data set that includes more than 100 rivers with discharge values ranging over four orders of magnitude. Comparatively, *Getirana and Peters-Lidard* [2013] obtained reliable RCs for 90 VSs from an initial data set of 444 because of convergence problems. In our study, convergence was achieved for all VSs before reaching the maximum number of iterations.

Hydrological information can be extracted from RC parameters. Here, we show how the RC parameters can be used to derive river bed elevations, Manning's roughness coefficient, and AMGH geomorphologic relationships.

Hydrologists mostly use water depth rather than the absolute elevation of the free surface. As explained above, the $Z_o$ parameter can be used to convert the elevation of the free surface into water depth. We compared the water depth from ADCP measurements at seven locations in the basin with the water depth obtained by subtracting "$Z_0$" from the altimetric water heights. The ADCP mean water depth was obtained by dividing the area by the width of the cross section, which was measured during the ADCP surveys and assuming that the river section had a rectangular shape, which is consistent with Manning's equation. The results for the seven test cases are shown in Table 9 with the distances between the ADCP measurement locations and the ENVISAT track that was used to make the comparison.

As seen in Table 9, the difference between the ADCP water depth (AWD) and estimated water depth (EWD) is mostly less than 10% of the ADCP water depth. The largest discrepancy was found at Itacoatiara, where the gauge and VS were more than 50 km apart. At the other locations, the absolute difference between the AWD and EWD ranged from 0 to 1.3 m (i.e., from zero to 6% of the AWD). These results confirm that the $Z_o$ parameter from our optimization process of the RC parameters can be considered a fair estimate of the river bed elevation; consequently, $Z_o$ can be used to convert the altimetric heights into water depths.

Additionally, we compared gauge stages, depths that were calculated from altimetric heights and $Z_0$, and depths that were estimated from the MGB model using statistical global relationships. Because gauges provide water stages that cannot be referenced to the bottom of the river rather than water depths, we fit the gauge series to the water depths derived from the altimetric series. The results from the four sites in the Madeira River Basin are presented in Figure 13. In all cases, the altimetry-derived water depths were more comparable with the gauge-derived water depths than the water depths in the MGB. At Nova Olinda do Norte (Figure 13a), the backwater influence of the Amazon River on the Madeira River is demonstrated. Because the Madeira River peaks between 2 and 3 months before the Amazon's main reach [*Meade et al.*, 1991], the water depth and stage after the peak are largely influenced by the water stage in the Amazon. Observations of water levels by satellite altimetry ensure that this behavior can be reproduced in our data.
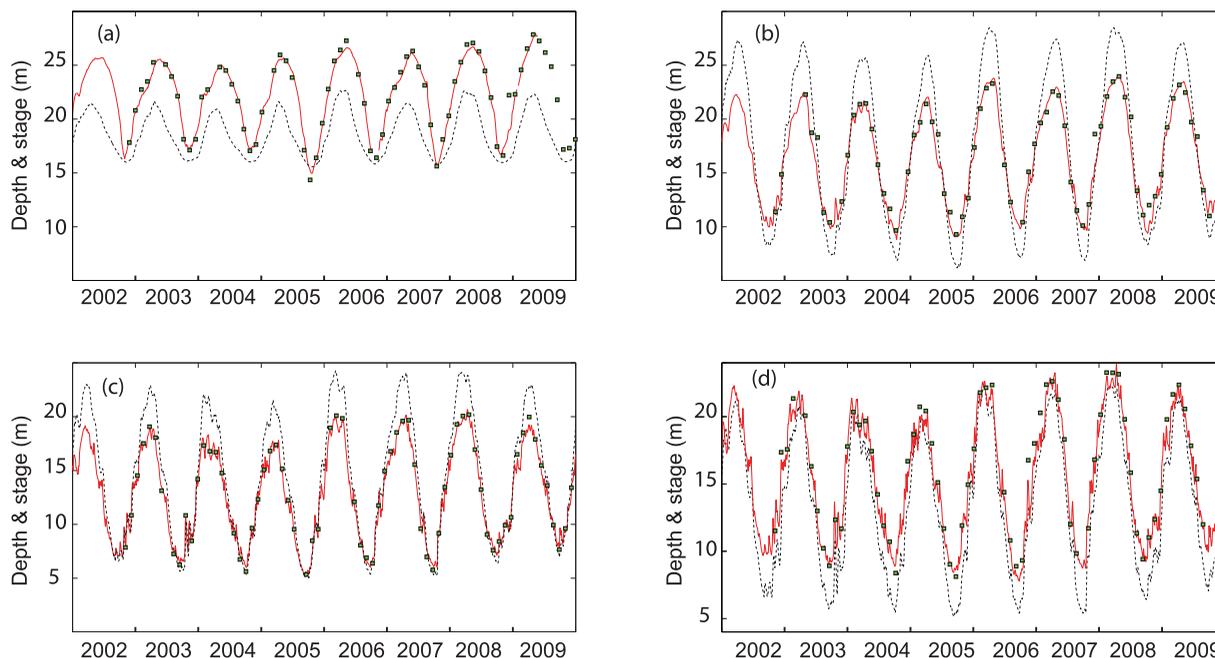
**Figure 13.** Time series of water depths and the stages at the following four gauge stations along the Madeira River: Nova Olinda do Norte (a), Manicoré (b), Porto Velho (c), and Abunã (d). The red line is the observed stage from ANA's website. The black broken line is the depth that was estimated by the MGB-IPH model at the nearest section. The black dots that are filled in green are the depths from the altimetric height series at crossings near the gauge and the "$Z_0$" parameter of their corresponding rating curve.

Conversely, the dynamics that are recorded in the gauge series were not fully reproduced by the MGB, which resulted in a significant time lag between the MGB and in situ peaks (see the decrease in the correlation between the in situ stages and MGB depths in Table 10) and a delayed recession limb. Figures 13b and 13c show that the geomorphologic laws used by *Paiva et al.* [2013a], which are the same laws used in many other models to describe river cross sections, do not provide accurate depth estimates everywhere. For Manicoré (Figure 13b) and Porto Velho (Figure 13c), the rated depth variations were comparable to the gauge stages variations when the range of the variations was overestimated in the MGB (Table 10). The bias between the stages and depths, regardless of whether they were rated or from the MGB, can be partially explained by the fact that the in situ stage represents the water depth from the zero of the gauge to the water surface. Hence, the water below the zero of the gauge was not considered. Thus, the rated depth is expected to be higher than the measured stage. One potential application of our study is to convert the stages that were recorded at the in situ gauges into actual water depths. The constrains included the fact that the VSs were located near the gauges and that the altimetry-derived depth series and in situ stage series varied the same way in amplitude and phase.

When the virtual and gauge stations did not share the same locations, the differences in the section widths between the gauge stations and VS (and thus the cross-sectional area differences) affected the in situ stage values and the MGB depths estimates. These differences can explain the positive bias between the rated depths and the in situ stages at Manicoré because the river passes through a narrower section that

**Table 10.** Benchmarking the Depth Estimates From Altimetry and MGB Compared With in Situ Stages[a]

| | Correlation (Pearson) | | Bias (m) | | Depth Range (m) | | |
| --- | --- | --- | --- | --- | --- | --- | --- |
| | Rated Depth | MGB Depth | Rated Depth | MGB Depth | In Situ | Rated Depth | MGB Depth |
| Nova Olinda | 0.9875 | 0.9085 | −7.20 | −3.56 | 12.37 | 13.50 | 6.99 |
| Manicoré | 0.9816 | 0.9877 | 2.04 | 1.46 | 14.88 | 14.67 | 22.10 |
| Porto Velho | 0.9977 | 0.9913 | −3.84 | −5.27 | 14.43 | 14.85 | 18.81 |
| Abuna | 0.9953 | 0.9850 | −3.04 | −0.68 | 14.69 | 15.16 | 16.80 |

[a]The MGB depths and in situ stages were obtained on the dates corresponding to those of the height time series from altimetry.
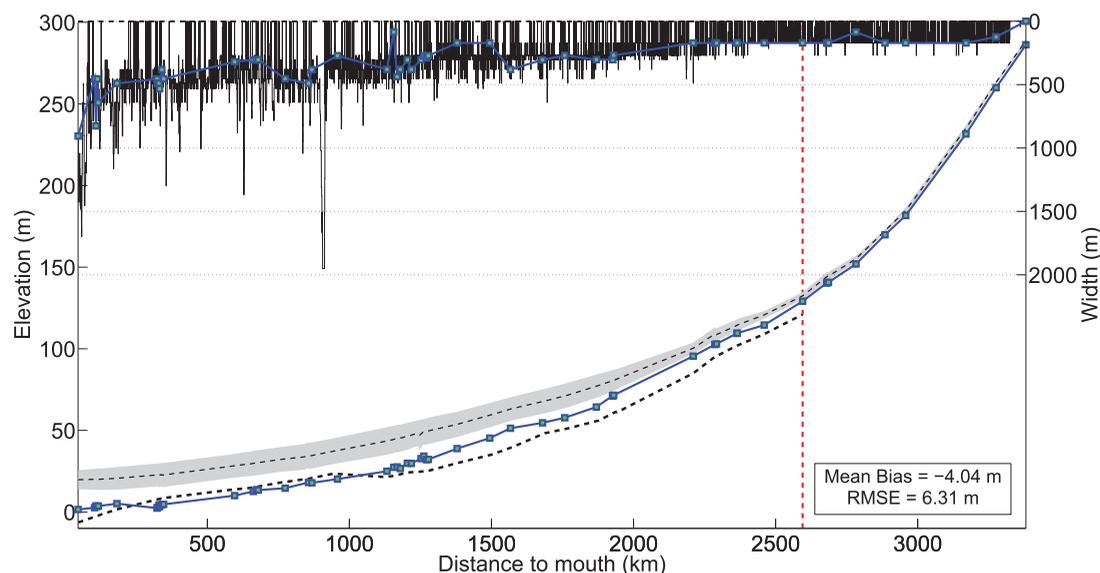
**Figure 14.** Comparison of the Purus River bottom level from the MGB (black broken line) and RC "$Z_0$" values (blue line with dots). The red broken line indicates the limits of the hydrodynamic model (e.g., where the model passed during its hydrological formulation). The gray area is delimited by the max/min water height values from satellite altimetry. The upper axes indicate the widths that were extracted from *Yamazaki et al.* [2014] along the river (black lines) and only at VS sites (blue line with dots).

corresponds with the measurement section. This variability could be considered in hydrological models (and particularly into the MGB-IPH) using more accurate width descriptors, such as the Global Width Database for Large Rivers [*Yamazaki et al.*, 2014]. Figure 13d illustrates that when the actual and estimated river widths are not significantly different (762 m in the MGB and 803 m in the GWD-LR) and result in almost equivalent section areas, the MGB and altimetry agree with the gauge stages, with the only bias resulting from the gauge set-up, as previously mentioned. The water depth estimates from the MGB-IPH model are sensitive to the river width and Manning's roughness coefficient at almost the same scale. In some individual cases, a wrong value of "$n$" could also result in the misevaluation of the water depth. We tested furthermore the possible impact of "n" in the MGB water depths estimates.

In Figure 14, we present the channel bottom from the MGB-IPH model and the RC parameter "$Z_0$" for the Purus River. The minimum and maximum water surface elevation lines were obtained from satellite altimetry. The widths were obtained from the database created by *Yamazaki et al.* [2014] extracted along the stream and at the VSs. In the MGB, the channel bottoms were derived by subtracting the mean depth derived from a global statistical rule of thumb based on the watershed area from the DEM elevation. We converted the SRTM orthometric heights of the river surfaces into EGM2008 values for geodetic consistency. A mean bias of approximately 4 m is visible between the two river bed profiles. Such a difference may result from the overvaluation of the necessary corrections that were applied to the SRTM DEM by *Paiva et al.* [2011]. Where no channel bottom information could be extracted from the MGB (i.e., where the model was run using the Musckingum-Cunge formulation), the RCs from the satellite altimetry could provide this information.

Together with widths from global data sets [e.g., *Yamazaki et al.*, 2014] and surface slopes from altimetry, the RC parameters provide a full description of the geometries of the streams. This description is necessary for inversion algorithms to provide initial discharge guesses for future missions, such as the SWOT mission.

As denoted by *Gleason and Wang* [2015], the range of discharges and AHG coefficients in a river must be large to observe AMHG relationships. Thanks to satellite altimetry, a large range of stations can be surveyed for a given river, resulting in a large range of hydraulic characteristics. We observed a relationship between the AHG coefficients using our methodology, as shown in Figure 6, which proves that the range of discharges obtained from satellite altimetry is large and validates the values of the RC parameters. One consequence of this method is that parameter values could be inferred along a river, which would provide discharge estimates at the VSs and at unmonitored sites.
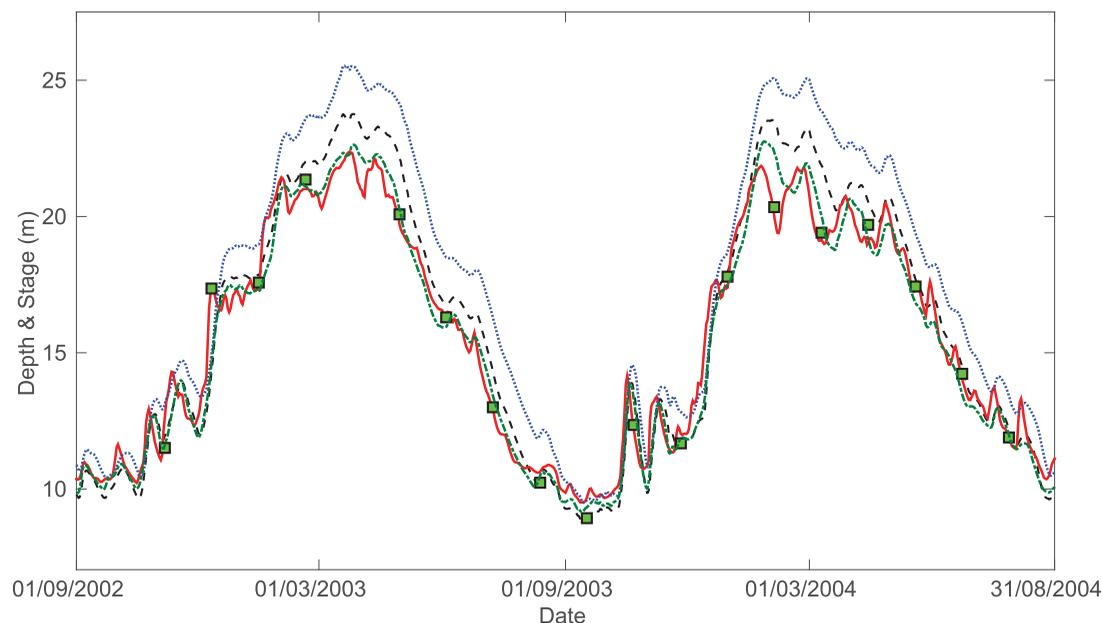
**Figure 15.** Comparison of depths that were estimated at Abunã through MGB-IPH with the original Manning's coefficient values from *Paiva et al.* [2013a] (black broken line), the increased "*n*" (blue line) and decreased "*n*" (red line), the rated depths from satellite altimetry and "$Z_0$" at the nearest VS (green squares), and the in situ stages at Abunã (black line).

The Manning's roughness coefficient, *n*, can be estimated from the leading parameter, *a*, if the reach width and surface slope are known independently. For example, the *n* value that we could estimate at SF-Purus-ENV-908 is 0.062 s/m$^{1/3}$ (using $a=27.737$, $B=218$ $m$, $S=0.000063$ $m/m$). We used the the hydraulic gradient line that resulted from the altimetric elevations to derive the slope, S. In addition, the river width was manually estimated from Landsat images. Using Yamazaki's database of river width [*Yamasaki et al.*, 2014], B = 272 m hence $n = 0.078$ s/m$^{1/3}$. According to Chow's classification [*Chow*, 1959], both values correspond to a sluggish river with pools and sandbanks, a description that is consistent with the average state of the Purus River at this location. Other preliminary evaluations of *n* were performed using the same method along the Amazon and Madeira Rivers. This process produced values of *n* that ranged from 0.015 to 0.17. These values are consistent with the values proposed by *Chow* [1959]. However, a small number of unrealistic values were discarded, particularly at VSs with an RC that was derived from low $E_{ns}$. Manning's roughness coefficient is a highly uncertain coefficient that is usually set at 0.03 and is considered fixed in most hydrological models. As we experienced during the above preliminary analysis, the value of *n* is derived from the RC parameter "*a*" with a large uncertainty (likely 100%), particularly because of the uncertainty of the river width. However, even with such a large uncertainty, large-scale variations can be detected and could be used for further modeling purposes.

As mentioned above, the MGB depths can be influenced by the value of Manning's roughness coefficient "*n*." We tested how changes in "*n*" affected depth estimates from the MGB-IPH. The model was run using the same configuration presented in this study, except for "*n*." This test was conducted for the Madeira sub-basin. First, we increased the initial value of *n* by 0.01 before reducing the value of *n* by 0.01. Figure 15 shows the changes in the depth estimates from the MGB-IPH model in these two configurations at Abunã. Both the depth range and phase were affected by changes in "*n*." The depths that were estimated by the MGB fit much better with the in situ stages and rated depths with reduced "*n*." Hence, we argue that the depths estimated from satellite altimetry and $Z_0$ coefficients can be used together with a more accurate width estimate to improve the "*n*" description in hydrological models, even when no in situ data are available.

Over 20 years of continuous water height monitoring has been conducted on continental water bodies, including precursor missions such as Topex/Poséidon and ERS2. Although these missions were originally designed for ocean monitoring, they can provide accurate water height estimates that can be converted to discharge estimates using RCs. This discharge time series can be updated in real time with incoming
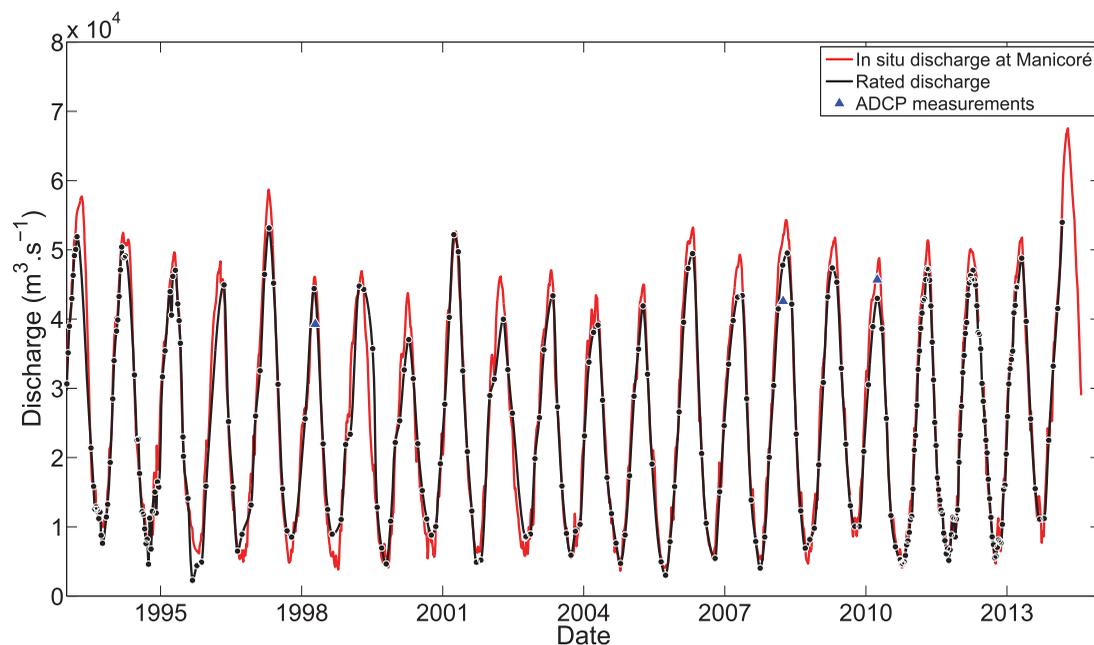
**Figure 16.** Hydrograph that shows the rated discharges from our rating curve and multimission altimetry at the ENVISAT groundtrack 235 and Jason-2 groundtrack 076 crossings with the Madeira River. The red line is the in situ discharge at the Manicoré gauge stations, which was calculated from stage observations and ANA's polynomial equation. The blue stars are three ADCP measurements that were obtained from ORE-HybAm (www.ore-hybam.org).

SARAL/AltiKa data. Figure 16 shows the discharge time series at a cross-over between ENVISAT pass 235 and Jason-2 pass 076. We used T/P (1993–1995), ERS2 (1995–2002), ENVISAT (2002–2010), Jason-2 (2010–2013), and SARAL (2013-ongoing) heights to calculate the discharge from the RC. In Figure 16, "observed discharges" refers to the discharge that was transformed using ANA's second-order polynomial relationship between stage observations and discharge. The ADCP measurements were taken from the ORE-Hybam database. The major flood discharge of the Madeira River that was observed at Manicoré was compared with the calculated discharge, and exhibited a mean absolute difference of less than 7% of the. At such locations, satellite altimetry could be used to perform climate change analysis and real-time monitoring of the hydrological cycle using SARAL and Jason-2 data and data from any other future altimetry mission.

## 6. Conclusions

We present and apply a global optimization method and RC formulation to predict river discharge from water elevations obtained using satellite altimetry over a large and poorly monitored basin, the Amazon Basin. This method was based on the SCEM-UA functional algorithm of optimization, the elevation of the free surface of the river according to the ENVISAT and Jason-2 satellite altimetric missions, and discharges that were predicted by the MGB-IPH rain-discharge model. RCs were successfully established for successive reaches of 100 rivers in the basin, with a mean discharge ranging from O 100 $m^3$/s to O 100,000 $m^3$/s.

Our method, which considers the uncertainties in the height and discharge series with a Monte-Carlo search for an optimal combination of RC parameters, provides confidence intervals for the rated discharges, which is key information that is rarely provided in discharge data sets. In situ discharges are mainly derived from stage readings via RCs that are established with more or less limited sets of actual discharge measurements. Our method could be applied to these in situ data so that the in situ discharges could be distributed with uncertainty estimates and better than rated or modeled discharges.

Our method was extended using analytical RC formulations that consider the temporal variations in the surface slope, particularly where the backwater effect is important. By including the local slope in the formulation of the RC at the confluences, we reproduced the loop in the height-discharge relationship and determined adequate discharge series with good $E_{ns}$ scores and reduced confidence intervals for the RC parameters.

Additionally, a net increase in performance indices, such as $E_{ns}$, and a decrease in the confidence intervals of the RC parameters from an RC formulation with and without slope variations can be used to identify the locations where such a backwater effect must be considered when predicting the discharge from the stage. These results anticipate the significant improvements that should occur with forthcoming altimetry missions, such as ICEsat-2 or SWOT, which should provide slope estimates with height measurements.

We showed that our RCs can be used with any altimetric series, regardless of the altimetry mission that was used to estimate the RC parameters. Therefore, these RCs can be used to predict the discharge at any VS whose series has been updated from a new mission, such as SARAL for the ENVISAT VSs or Jason-3 for the Jason-2 VSs. Applying this process to former missions, such as ERS-2 for the ENVISAT VSs and Topex/Poséidon for the Jason-2 VSs, when the altimetric measurements of these missions will be fully reprocessed will extend the series back to the early 1990s. All of these series will be continued with the forthcoming wide swath mission SWOT, which is scheduled for launch in 2020 and which will cover the ground tracks of any nadir mission.

The Içá and Japura Rivers, where no satisfactory RCs were estimated, suggest that our method can be used to identify concerns with discharges that are simulated by models. Indeed, these cases indicate how sensitive the performance coefficients are with respect to the quality of the discharge data. Large uncertainties in the RC parameters can increase concerns regarding the quality of the discharge series. Globally, altimetry and associated RCs can be used to assess the performances of discharge simulations. These performance assessments of model runs are commonly based on comparisons with in situ discharge series. Altimetry is another completely independent and widespread data set source that significantly enlarges the possible validation data set, particularly in poorly monitored basins.

Our method provides access to vertically referenced river bed elevations and, consequently, river depths. River bed elevation information is rare for poorly gauged basins. Hydrological models usually use river bed elevations derived from geomorphologic equations and a digital elevation model (DEM) to compensate for this lack of in situ information. However, our bed elevations can be used for these models. In addition, using river bed elevations that are measured in this way will ensures consistency in terms of altitudinal referencing if the hydrological model also includes satellite altimetry, such as models with assimilation modes.

When applicable, the RC parameters were accurate enough to support the AMGH geomorphological rules that were highlighted by *Gleason et al.* [2015]. The present data set of river bed elevations and the (a, b) pairs that suggest possible AMGH relationships along successive river reaches can be associated with other global data sets such as the global widths data set GWD-LR by *Yamasaki et al.* [2014] to play an important role in the preparation of future missions, such as SWOT, for the automatic prediction of discharge from space.

The method developed in this study provides a more accurate method for deriving hydrological parameters than methods proposed in previous studies regarding the prediction of discharge from altimetric heights. For example, the equivalent Manning's roughness coefficient calculated for SF-Purus-ENV-908 was consistent with the ranges provided by *Chow* [1959]. This estimation of a local equivalent Manning's roughness coefficient requires that the width of the reach is known independently. However, the Manning's coefficient is difficult to measure in situ. Consequently, this factor is commonly derived from tables when needed in hydrological or hydrodynamical models. Large variations in Manning's coefficient can be inferred for further modeling by combining the *a* parameter of the RC and the mean section width.

## References

Alsdorf, D., E. Rodríguez, and D. P. Lettenmaier (2007), Measuring surface water from space, *Rev. Geophys.*, *45*, RG2002, doi:10.1029/2006RG000197.

Birkett, C. M., L. A. K.Mertes, T. Dunne, M. H. Costa, and M. J. Jasinski (2002), Surface water dynamics in the Amazon Basin: Application of satellite radar altimetry, *J. Geophys. Res.*, *107*(D20), 8059, doi:10.1029/2001JD000609.

Birkinshaw, S. J., G. M. O'Donnell, P. Moore, C. G. Kilsby, H. J. Fowler, and P. A. M. Berry (2010), Using satellite altimetry data to augment flow estimation techniques on the mekong river, *Hydrol. Processes*, *24*(26), 3811–3825.

Birkinshaw, S. J., P. Moore, C. Kilsby, G. M. O'Donnell, A. Hardy, and P. A. M. Berry (2014), Daily discharge estimation at ungauged river sites using remote sensing, *Hydrol. Processes*, *28*(3), 1043–1054.

Bjerklie, D. M., S. L. Dingman, C. J. Vorosmarty, C. H. Bolster, and R. G. Congalton (2003), Evaluating the potential for measuring river discharge from space, *J. Hydrol.*, *278*, 17–38.

Calmant, S., and F. Seyler (2006), Continental sufrace water from satellite altimetry, *C. R. Geosci.*, *338*(14–15), 1113–1122, doi:10.1029/2001JD000609.

Calmant, S., F. Seyler, and J. F. Cretaux (2008), Monitoring continental surface waters by satellite altimetry, *Surv. Geophys.*, *29*, 247–269.

Calmant, S., J. Santos da Silva, D. Medeiros Moreira, F. Seyler, C. K. Shum, J.-F. Crétaux, and G. Gabalda (2012), Detection of ENVISAT RA2/ICE-1 retracked Radar Altimetry Bias over the Amazon Basin Rivers using GPS, *Adv. Space Res.*, *51*(8), 1551–1564, doi:10.1016/j.asr.2012.07.033.

Chow, V. T. (1959), *Open-Channel Hydraulics*, 680 pp., McGraw-Hill, N. Y.

Chow, V. T., D. R. Maidment, and L. W. Mays (1988), *Applied Hydrology*, 572 pp., McGraw-Hill, N. Y.

Clarke, R. T. (1999), Uncertainty in the estimation of mean annual flood due to rating-curve indefinition, *J. Hydrol.*, *222*(1–4), 185–190.

Clarke, R. T., E. M. Mendiondo, and L. C. Brusa (2000), Uncertainties in mean discharges from two large South American rivers due to rating curve variability, *Hydrol. Sci. J.*, *45*(2), 221–236.

Collischonn, W., D. G. Allasia, B. C. Silva, and C. E. M. Tucci (2007), The MGB-IPH model for large-scale rainfall-runoff modeling, *Hydrol. Sci. J.*, *52*, 878–895.

Dingman, S. L., and D. M. Bjerklie (2005), Hydrological application of remote sensing: Surface fluxes and other derived variables-river discharge, in *Encyclopedia of Hydrological Sciences*, edited by M.G. Anderson, John Wiley, N. Y.

Dingman, S. L., and K. P. Sharma (1997), Statistical development and validation of discharge equations for natural channels, *J. Hydrol.*, *199*, 13–35.

Dubey, A. K., P. K. Gupta, S. Dutta, and R. P. Singh (2015), An improved methodology to estimate river stage and discharge using Jason-2 satellite data, *J. Hydrol.*, *529*(3), 1776–1787, doi:10.1016/j.jhydrol.2015.08.009.

Durand, M., J. Neal, E. Rodríguez, K. M. Andreadis, L. C. Smith, and Y. Yoon (2014), Estimating reach-averaged discharge for the River Severn from measurements of river water surface elevation and slope, *J. Hydrol.*, *511*, 92–104, doi:10.1016/j.hydrol.2013.12.050.

Farr, T. G., et al. (2007). The shuttle radar topography mission, *Rev. Geophys.*, *45*, RG2004, doi:10.1029/2005RG000183.

Finsen, F., C. Milzow, R. Smith, P. Berry, and P. Bauer-Gottwein (2014), Using radar altimetry to update a large-scale hydrological model of the Brahmaputra river basin, *Hydrol. Res.*, *45*(1), 148–164.

Frappart, F., S. Calmant, M. Cauhope, F. Seyler, and A. Cazenave (2006), Preliminary results of Envisat RA-2-derived water levels validation over the Amazon basin, *Remote Sens. Environ.*, *100*, 252–264, doi:10.1016/j.rse.2005.10.027.

Garambois, P.-A., and J. Monnier (2015), Inference of effective river properties from remotely sensed observations of water surface, *Adv. Water Resour.*, *79*, 103–120, doi:10.1016/j.advwatres.2015.02.007.

Gelman, A., and D. B. Rubin (1992), Inference from iterative simulation using multiple sequences, *Stat. Sci.*, *7*, 457–472.

Getirana, A. C. V., and C. Peters-Lidard (2013), Water discharge estimates from large radar altimetry data sets in the Amazon basin, *Hydrol. Earth Syst. Sci. Discuss.*, *9*, 7591–7611, doi:10.5194/hessd-9-7591-2013.

Getirana, A. C. V., M.-P. Bonnet, E. Roux, S. Calmant, O. C. Rotunno Filho, and W. J. Mansur (2009), Hydrological monitoring of large poorly gauged basins: A new approach based on spatial altimetry and distributed rainfall–runoff model, *J. Hydrol.*, *379*, 205–219, doi:10.1016/j.jhydrol.2009.09.049.

Gleason, C. J., and L. C. Smith (2014), Toward global mapping of river discharge using satellite images and at-many-stations hydraulic geometry, *Proc. Natl. Aacd. Sci. U. S. A.*, *111*(13), 4788–4791, doi:10.1073/pnas.1317606111.

Gleason, C. J., and J. Wang (2015), Theoretical basis for at-many-stations hydraulic geometry, *Geophys. Res. Lett.*, *42*, 7107–7114, doi:10.1002/2015GL064935.

Gleason, C. J., L. C. Smith, and J. Lee (2015), Retrieval of river discharge solely from satellite imagery and at-many-stations hydraulic geometry: Sensitivity to river form and optimization parameters, *Water Resour. Res.*, *50*, 9604–9619, doi:10.1002/2014WR016109.

Herschy, R. W. (1999). The evaluation of errors at flow measurement stations, in *International Symposium on Hydrometry, Koblenz, Germany, IAHS Publ.*, *99*, 109–131.

ISO 1100-2 (1998), Measurement of liquid flow in open channels—Part 2: Determination of the stage-discharge relation, *International Organization for Standardization*, Geneva, Switzerland.

Jaccon, G. (1987), Jaugeage de l'Amazone à Obidos par les methods du bateau mobile et des grands fleuves, *Hydrol. Cont.*, *2*(2), 117–126.

Jasinski, M. J., C. M. Birkett, S. Chinn, and M. H. Costa (2001), Feasibility of estimating Amazon river stahe and discharge using Topex/Poseidon altimetric data, in Land Surface Hydrology Program, Abstract pressented at NASA/NOAA GAPP and Hydrology Principal Investigadors Meeting, Potomac, Md., 30 Apr–May, Global Energy and Water Cycle Experiment.

Kouraev, A. V., E. A. Zakharova, O. Samain, N. M. Mognard, and A. Cazennave (2005), Ob' River discharge from Topex-Poséidon satellite altimetry (1992-2002), *Remote Sens. Environ.*, *93*, 238–245.

Lambie, J. C. (1978), Measurment of flow: Velocity-area methods, in *Hydrometry: Principles and Practices*, edited by R. W. Herschy, John Wiley, Chichester, West Sussex, U. K.

Leon, J. G., S. Calmant, F. Seyler, M. P. Bonnet, M. Cauhope, F. Frappart, and N. Filizola (2006), Rating curves and estimation of average water depth at the Upper Negro River based on satellite altimeter data and modelled discharges, *J. Hydrol.*, *328*(3-4), 481–496.

Manning, R. (1891), On the flow of water in open channels and pipes, *Trans. Inst. Civ. Eng. Ire.*, *20*, 161–207.

McMillan, H., J. Freer, F. Pappenberger, T. Krueger, and M. Clark (2010), Impacts of uncertain river flow data on rainfall-runoff model calibration and discharge predictions, *Hydrol. Processes*, *24*(10), 1270–1284.

Meade, R. H., J. M. Rayol, S. C. da Conceicaõ, and J. R. G. Natividade (1991), Backwater effects in the Amazon River Basin of Brazil, *Environ. Geol. Water Sci.*, *18*(2), 105–114.

Michailovsky, C. I., S. McEnnis, P. A. M. Berry, R. Smith, and P. Bauer-Gottwein (2012), River monitoring from satellite radar altimetry in the Zambezi River basin, *Hydrol. Earth Syst. Sci.*, *16*, 2181–2192, doi:10.5194/hess-16-2181-2012.

Moramarco, T., and V. P. Singh (2001), Simple method for relating local stage and remote discharge, *J. Hydrol. Eng.*, *6*(1), 78–81.

Moramarco, T., S. Barbetta, F. Melone, and V. P. Singh (2005), Relating local stage and remote discharge with significant lateral inflow, *J. Hydrol. Eng.*, 10(1), 58–69.

Moyeed, R. A., and R. T. Clarke (2005), The use of Bayesian methods for fitting rating curves, with case studies, *Adv. Water Resour.*, *28*, 807–818.

Nash, J., and J. V. Sutcliffe (1970), River flow forecasting through conceptual models part I-A discussion of principles, *J. Hydrol.*, *10*(3), 282–290.

Paiva, R. C. D., W. Collischonn, and C. E. M. Tucci (2011), Large scale hydrologic and hydrodynamic modeling using limited data and a GIS based approach, *J. Hydrol.*, *406*, 170–181.

Paiva, R. C. D., D. C. Buarque, W. Collischonn, M.-P. Bonnet, F. Frappart, S. Calmant, and C. A. B. Mendes (2013a), Large scale hydrologic and hydrodynamic modeling of the Amazon River basin, *Water Resour. Res.*, *49*, 1226–1243, doi:10.1002/wrcr.20067.

Paiva, R. C. D., W. Collischonn, M.-P. Bonnet, L. G. G. de Gonçalves, S. Calmant, A. Getirana, and J. Santos da Silva (2013b), Assimilating in situ and radar altimetry data into a large-scale hydrologic-hydrodynamic model for streamflow forecast in the Amazon, *Hydrol. Earth Syst. Sci.*, *17*, 2929–2946, doi:10.5194/hess-17-2929-2013.

Paiva, R. C. D., W. Collischonn, and D. C. Buarque (2013c), Validation of a full hydrodynamic model for large scale hydrologic modelling in the Amazon, *Hydrol. Processes*, *27*(3), 333–346, doi:10.1002/hyp.8425.

Papa, F., F. Durand, W. B. Rossow, A. Rahman, and S. K. Bala (2010), Satellite altimeter-derived monthly discharge of the Ganga-Brahmaputra River and its seasonal to interannual variations from 1993 to 2008, *J. Geophys. Res.*, *115*, C12013, doi:10.1029/2009JC006075.

Pavlis, N. K., S. A. Holmes, S. C. Kenyon, and J. K. Factor (2012), The development and evaluation of the Earth Gravitational Model 2008 (EGM2008), *J. Geophys. Res.*, *117*, B04406, doi:10.1029/2011JB008916.

Petersen-Øverleir, A., and T. Reitan (2005), Objective segmentation in compound rating curves, *J. Hydrol.*, *311*(1–4), 188–201.

Potter, K.W., and J. F. Walker (1985), An empirical study of flood measurement error, *Water Resour. Res.*, *21*(3), 403–406.

Rantz, S. E., et al. (1982). Measurement and computation of streamflow, vol. 1, measurement of stage and discharge, *U. S. Geol. Surv. Water Supply Pap. 2175*, 284 pp.

Santos da Silva, J., S. Calmant, F. Seyler, O. C. Rotunno Filho, G. Cochonneau, and W. J. Mansur (2010), Water levels in the Amazon basin derived from the ERS 2 and ENVISAT radar altimetry missions, *Remote Sens. Environ.*, *114*(10), 2160–2181.

Santos da Silva, J., S. Calmant, F. Seyler, H. Lee, and C. K. Shum (2012), Mapping of the Extreme Stage variations using ENVISAT altimetry in the Amazon basin Rivers, *Int. Water Tech. J.*, *2*(1), 14–25.

Santos da Silva, J., S. Calmant, F. Seyler, D. Medeiros Moreira, D. Oliveira, and A. Monteiro (2014), Radar Altimetry aids Managing gauge networks, *Water Resour. Manage.*, *28*(3), 587–603.

Seyler, F., S. Calmant, J. Santos da Silva, D. Medeiros Moreira, F. Mercier, and C. K. Shum (2013), From Topex/Poséidon to Jason-2/OSTM in the Amazon basin, *Adv. Space Res.*, *51*(8), 1542–1550, doi:10.1016/j.asr.2012.11.002.

Tarpanelli, A., S. Barbetta, L. Brocca, and T. Moramarco (2013), River discharge estimation by using altimetry data and simplified flood routing modeling, *Remote Sens.*, *5*(9), 4145–4162.

Tomasella, J., L. S. Borma, J. A. Marengo, D. A. Rodriguez, L. A. Cuartas, C. A. Nobre, and M. C. R. Prado (2010), The droughts of 1996-97 and 2004-05 in Amazonia: Hydrological response in the river main-stem, *Hydrol. Processes*, *25*(8), 1228–1242.

Vrugt, J. A., H. V. Gupta, W. Bouten, and S. Sorooshian (2003), A Shuffled Complex Evolution Metropolis algorithm for optimization and uncertainty assessment of hydrologic model Parameters, *Water Resour. Res. 39*(8), 1201, doi:10.1029/2002WR001642.

Vörösmarty, C. J., P. Green, J. Salisbury, and R. B. Lammers (2000), Global water resources: Vulnerability from climate change and population growth, *Science*, *289*, 284–288.

Yamazaki, D., F. O'Loughlin, M. A. Trigg, Z. F. Miler, T. M. Pavelsky, and P. D. Bates (2014), Development of the global width database for large rivers, *Water Resour. Res.*, *50*, 3467–3480, doi:10.1002/2013WR014664.

Zakharova E. A., A. V. Kouraev, A. Cazenave, and F. Seyler (2006), Amazon River discharge estimated from Topex/Poséidon altimetry, *C. R. Geosci.*, *338*(3), 188–196.

## Erratum

In the originally published version of this article, a sentence on page 3789 erroneously cited the wrong source. The correct sources have been added to the References List and the sentence has been updated. This version may be considered the authoritative version of record.